Chapter

Crystal Facet Engineering of TiO_2 from Theory to Application

Szymon Dudziak, Marta Kowalkińska and Anna Zielińska-Jurek

Abstract

Recently, the surface structure effect on photocatalytic activity has gathered increasing attention due to its reported influence on the charge carrier trapping and separation. Detailed control over the surface structure can be achieved by exposing the specific crystal facets. As a result, the photogenerated electrons and holes can be effectively separated between the different facets of semiconductor crystals. TiO_2 is the most studied photocatalyst, with the particles exposing {0 0 1}, {1 0 0}, {1 0 1}, {1 1 0}, {1 1 1}, and {1 0 5} crystal facets. The performed studies have shown that the efficiency of the photocatalytic process strongly depends on the nature of the crystal facet exposed at the photocatalyst surface. In this regard, this chapter focuses on the comparison of possible surface-related parameters and photocatalytic activity of anatase, rutile, and brookite polymorphs with exposed different crystal facets. Particularly, computational data on their different possible surface structures are summarized, focusing on the geometry, energy, and possible reconstructions. This is followed by the general description of the hypothetical Wulff constructions and existing stabilization/synthesis strategies. Such an approach could help to further design, simulate, and optimize photocatalyst surface for efficient photoreduction and photooxidation processes.

Keywords: crystal facets, computational, titanium dioxide, photocatalysis, crystal growth, surface engineering

1. Introduction

Titanium dioxide (TiO_2) is one of the most studied photocatalysts, especially considering its application in the photocatalytic degradation of micropollutants. TiO_2 can induce specific redox reactions through photogenerated charge carriers in photocatalysis. Such process can be divided into subsequent steps, including (1) excitation of electrons in the TiO_2 structure; (2) dissociation of the generated excitons to free electrons and holes; (3) migration of the charge carriers to the surface; and (4) transfer of the e^- or h^+ to substrate present at the surface. All of these steps are common for every photocatalytic reaction, and each deals with limitations that influence the overall process efficiency. However, steps (3) and (4) occur at the surface. Therefore, any change at the interface between the photocatalyst and a substrate can

induce significant changes in the involved elementary reactions. The importance of this interface and photocatalyst surface was realized very early in the photocatalytic studies, discussing problems like surface polarization with excess electrons, modification with noble metals, and surface complexation with bidentate benzene derivatives to improve the transfer of the charge carriers [1–3]. Simultaneously, the challenges of surface trapping and recombination of the generated charge carriers were also highlighted.

However, concerning these early studies, the exact geometry of the photocatalyst surface was not considered at this point, and ultrafine particles were studied without well-defined geometry. In the last years, significant progress has been made both in the preparation procedures of the TiO_2 particles and in the application of computational methods to simulate the geometry and properties of such interfaces at the atomic scale. As a result, stabilization of a specific interface structure can be achieved during the photocatalyst preparation, leading to the formation of faceted particles terminated with specific, well-defined crystal planes. At present, the application of such single-crystalline particles can be considered a state-of-the-art approach for investigating the details of photocatalytic reactions. Moreover, when systematically studied, it allows for the optimization of the final structure of the photocatalyst and increases its activity in a specific reaction [4]. This is primarily a result of a preferred electronic structure of the exposed facet. Therefore, photogenerated electrons and holes may accumulate at different crystal facets leading to improved charge carriers' separation and more selective photocatalytic reactions. In this regard, this chapter concisely highlights recent state-of-the-art progress in (1) the synthesis of crystal-facet exposed anatase, rutile, and brookite, (2) crystal facet-dependent properties of TiO_2, and (3) the correlation of surface properties with photocatalytic activity in photodegradation of emerging pollutants present in water, H_2 generation, and CO_2 reduction into valuable chemicals. Furthermore, by reviewing the research progress on crystal facet engineering of TiO_2, we hope to provide directions for future selective semiconductor modification with electron-donor or electron-acceptor to improve the overall efficiency in photocatalytic reaction kinetics and mechanism.

2. Computed geometries and energies of the TiO_2 surfaces in vacuum

Recently, detailed atomic structures of the possible crystal facet terminations and their corresponding surface energies are preferably studied using a computational approach. This allows us to describe actual surface geometry and investigate how it will change in a different environment. Therefore, energetic stabilization of the specific facet might be predicted to help obtain it experimentally. However, the analyzed models are often studied in a vacuum, which enables researchers to compare the relative stability of different structures and provides a useful starting point for further investigations. Concerning TiO_2 crystal planes, corresponding surface models were analyzed in detail for both anatase and rutile polymorphs, including (0 0 1), (1 0 0), (1 0 1), (1 0 3), (1 0 5), (1 1 0), and (1 1 2) structures for anatase [5–11], as well as (0 0 1), (0 1 1), (1 0 0), (1 1 0), and (1 1 1) for rutile [10–14]. On the other hand, brookite surfaces are rarely investigated. Nevertheless, a detailed study on different brookite surfaces was reported by Gong and Selloni [15], as well as additional information can be found about the (1 0 1), (1 2 1), and (2 0 1) structures [16]. Moreover, in the case of some models, different atomic geometries or possible reconstructions have been suggested. This specifically includes (1 x 4) reconstruction of the anatase (0 0 1)

surface, reconstruction of the rutile (0 0 1), (0 1 1), and (1 0 0) surfaces, as well as two possible geometries of anatase (1 0 3), including smooth $(1\ 0\ 3)_s$ and faceted $(1\ 0\ 3)_f$ terminations. The following description is a summation of these works. Finally, a different number of atoms exposed to the environment are discussed for different surfaces. For example, atoms from the second (or deeper) atomic layer are not always considered as "exposed" by the authors, although they are needed to complete surface structure. Here, if the surface structure has visible steps that give possible access to such atoms, we have always considered them as exposed ones. Nevertheless, it should be minded that such atoms are more or less covered with the ones located closer to the top of the surface and might be less accessible in practice.

2.1 Unreconstructed anatase surfaces

The atomic structures of the perfect anatase terminations with different crystal planes are presented in **Figure 1**. Starting from the top-left side, the (0 0 1) surface is

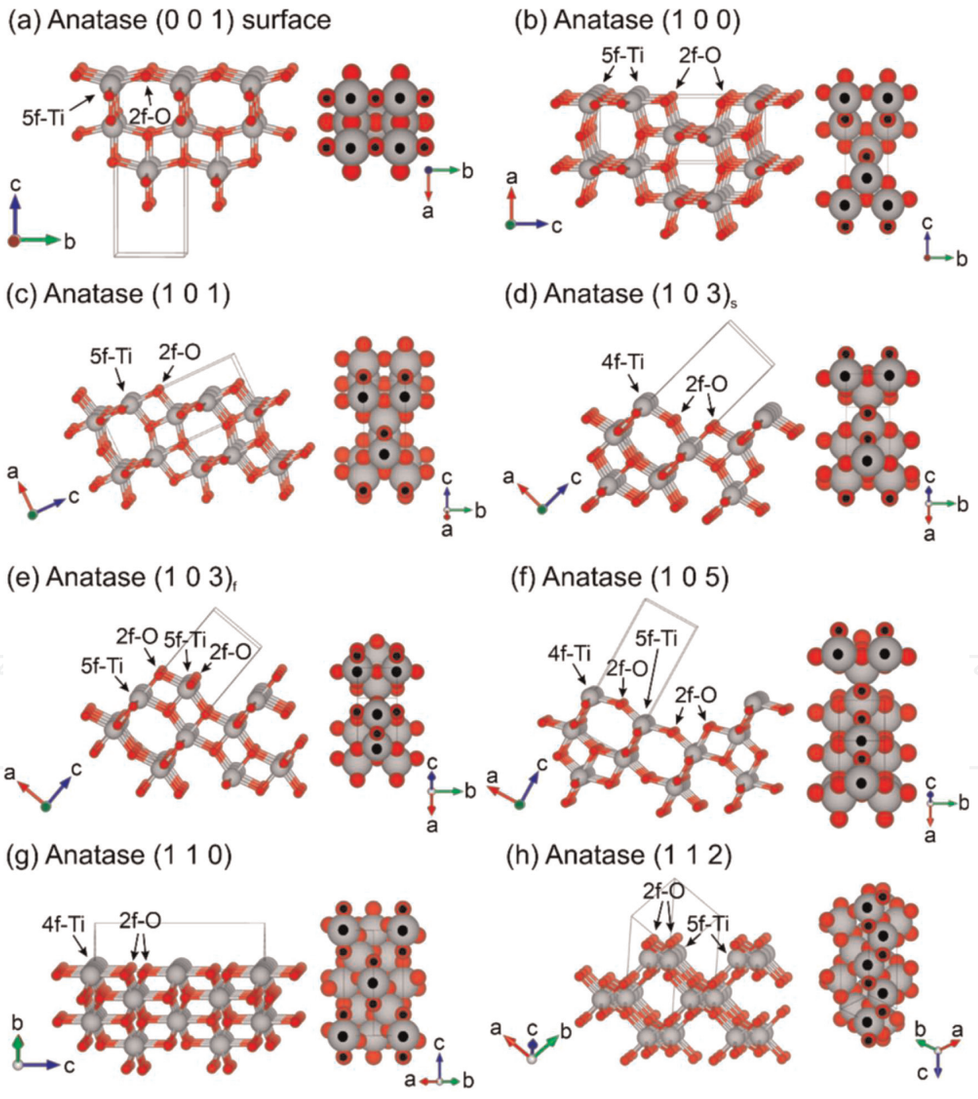

Figure 1.
Perfect, bulk-cut atomic geometries of different anatase surfaces in their isomeric (ball-and-stick models) and top (space-filling models) views. Ti atoms are large, gray spheres and O atoms are small red ones. In the top view, the undercoordinated atoms are marked with dots. The bulk crystal unit cell and the unit cell vectors are presented to help navigate between different structures. Visualizations were performed with the VESTA program.

flat, exposing all of the Ti atoms as 5-fold coordinated sites (5f-Ti) and ½ of the O as 2-fold coordinated ones (2f-O). The high density of the undercoordinated species leads to a high surface energy of about 0.90–1.08 $J \cdot m^{-2}$. Noticeable relaxation of the atomic structure, compared to the bulk (0 0 1) crystal plane, includes breaking of the bond symmetry between 5f-Ti and two neighboring 2f-O, resulting in one Ti-O bond being visibly longer than the other. For the (1 0 0) surface, exposed atoms consist of both undercoordinated 5f-Ti and 2f-O, as well as fully coordinated 6f-Ti and 3f-O. Here, all Ti atoms exposed directly at the first atomic layer are 5f-coordinated, while only ½ of oxygens are 2f-coordinated, as shown in **Figure 1b**. Moreover, visible steps inward of the crystal structure give access to the second-layer atoms, which are always fully coordinated. Including these sites as surface, atoms give a final fraction of 5f-Ti is ½ and 2f-O is ⅓. The relaxed structure of the (1 0 0) facet shows outward relaxation of fully coordinated O atoms and inward relaxation of 5f-Ti, creating an oxygen-rich interface, while 6f-Ti relaxes outward. Corresponding surface energy is usually reported in the range of 0.53 to 0.79 $J \cdot m^{-2}$.

Furthermore, the (1 0 1) surface of anatase is energetically the most stable, with the reported surface energy in a vacuum being 0.44–0.65 $J \cdot m^{-2}$, and it is commonly observed in nature. The corresponding atomic structure consists of a sawtooth profile with ½ of Ti atoms being 5f-coordinated and ⅓ of O atoms being 2f-coordinated, as shown in **Figure 1c**. Here, the most exposed atoms are undercoordinated oxygens, and specifically, further relaxation leads to the outward rise of the 3f-O above the undercoordinated Ti. Similarly to the (1 0 0) surface, the (1 0 1) can be considered oxygen-rich. Next, the (1 0 3) surface is often discussed in two possible terminations, either smooth one $(1\ 0\ 3)_s$ or faceted $(1\ 0\ 3)_f$, both presented in **Figure 1d**-**e**, respectively. The smooth (1 0 3) termination is one of the few facets that exposes 4-fold coordinated Ti atoms (4f-Ti) at the top of the surface, being ⅓ of the total surface Ti. Other Ti sites located below the 4f-Ti "tooth" are fully coordinated. Here, the 2f-O represents ⅖ of all exposed O and two 2f-O are always bonded to the single 6f-Ti. The outermost O atoms are 3f-coordinated and, similar to other facets, undergo significant relaxation outward of the crystal structure. On the contrary, on the faceted (1 0 3) termination relatively large fraction of Ti atoms is 5f-coordinated, being ⅔ of all Ti. Two different 5f-Ti sites exist on this surface, one bonded to a single 2f-O and the other bonded to three 2f-O atoms. The total fraction of 2f-O is the same as for the smooth (1 0 3), that is, ⅖. Similar to the (0 0 1) surface, significant symmetry breaking is observed for the 2f-O bridging two equivalent 5f-Ti sites (the one bonded to three 2f-O), resulting in one bond being longer than the other. Analogically to other facets, 3f-coordinated O relaxes outward; however, the change is smaller than for a $(1\ 0\ 3)_s$ structure. Energetically, Lazzeri et al. reported that the $(1\ 0\ 3)_f$ is slightly more stable than $(1\ 0\ 3)_s$, with surface energies being 0.83 and 0.93 $J \cdot m^{-2}$, respectively [5]. However, different results were presented by Zhao et al. with analogical energies of 1.14 and 1.05 $J \cdot m^{-2}$ [6].

The (1 0 5) surface structure is rarely discussed; however, Jiang et al. have proposed possible geometry of such facet with a corresponding surface energy of 0.84 $J \cdot m^{-2}$. In their model, the atomic structure of the (1 0 5) facet composes of both 4f-Ti (¼) and 5f-Ti (¼) exposed, together with 2f-O ($^3/_7$), as shown schematically in **Figure 1f** [17]. Although performed, relaxation of the geometry was not described. Furthermore, the (1 1 0) surface has a characteristic layered structure with deep cavities running along the [0 0 1] direction. Such structure exposes up to four atomic Ti layers and three O layers at different depths. As shown in **Figure 1g**, the first layer composes only of 4f-Ti and 2f-O atoms, while further layers are fully coordinated. As

described by Zhao et al., this surface also shows a "layered" relaxation pattern, where O atoms relax outward for the odd-numbered letters and inward for the even-numbered ones [6]. Simultaneously, Ti relaxes in the opposite pattern, ultimately leading to the breaking of the perfect 2D symmetry of the surface structure (i.e., the surface stops being perfectly flat, in contrast to the bulk crystal plane). Following this description and maximum exposition of the first four Ti and first three O layers, the fraction of undercoordinated species is ¼ for 4f-Ti and ⅓ for 2f-O. Corresponding surface energy is commonly reported between 01.02 and 1.33 $J \cdot m^{-2}$.

Finally, the (1 1 2) surface is also rarely considered; however, Mino et al. analyzed its surface model with surface energy between 0.95 and 0.98 $J \cdot m^{-2}$, depending on the possible relaxation of the cell parameters (exact value was approximated by the authors from the graph) [9]. Similar to the (1 1 0) surface, the (1 1 2) geometry exposes the first layer of undercoordinated species (5f-Ti and 2f-O, both being ½ of all Ti/O atoms) and the second layer of fully coordinated atoms, as shown in **Figure 1h**. A detailed relaxation pattern was not described.

2.2 Unreconstructed rutile surfaces

Concerning the rutile crystal structure of TiO_2, its possible terminations with different crystal planes are shown in **Figure 2**, analogically to the anatase. Starting from the (0 0 1) crystal plane, the corresponding termination shows structure similar to anatase (1 1 0), with the first atomic layer composed fully of undercoordinated 4f-Ti and 2f-O species and the second layer being fully coordinated. Assuming that the second layer is also partially exposed to the environment, the final fraction of undercoordinated sites is again ½ for both Ti and O. The relaxation of this surface is also similar to that of anatase (1 1 0), where the 4f-Ti atoms on the surface relax inward toward the bulk structure, while the 2f-O and 6f-Ti atoms relax outward. The high density of the broken bonds results in high surface energy, with reported values between 1.21 and 1.58 $J \cdot m^{-2}$, making it one of the least stable rutile facets. Furthermore, **Figure 1b** shows (0 1 1) surface structure of the rutile phase with a little corrugated profile. Here, the uppermost part composes fully of 5f-Ti and 2f-O, while subsurface 3f-O atoms are also partially exposed, ultimately being ½ of all O atoms. Surface relaxation described by Barnard et al. showed that all 5f-Ti, 2f-O, and 3f-O atoms relax outward on this surface; however, a bit different pattern was also reported by Ramamoorthy et al. [14]. Along the (0 0 1) surface, the (0 1 1) is reported to be one of the least stable rutile surfaces, with surface energies reported in the range of 0.95 to 1.11 $J \cdot m^{-2}$.

Furthermore, the (1 0 0) surface shows a layered structure with rows of 5f-Ti and 2f-O atoms at the top of the exposed "tooths," as well as fully coordinated species in the cavities. The corresponding fraction of the undercoordinated atoms is ½ for Ti and ⅓ for O. Relaxation pattern described by Ramamoorthy et al. includes the moving of the surface Ti and O atoms in opposite directions along the [0 1 0] axis [14]. Simultaneously, surface Ti relaxes outward the crystal structure. Corresponding surface energy was reported in the range between 0.60 and 0.83 $J \cdot m^{-2}$. Next, the (1 1 0) structure is energetically the most stable surface of the rutile polymorph, with the reported surface energy between 0.34 and 0.59 $J \cdot m^{-2}$. Its surface structure exposes both 5f-Ti atoms (½) and 2f-O (⅓) in the subsequent rows, as presented schematically in **Figure 2d**. Relaxation of the (1 1 0) structure includes an inward shift of all the undercoordinated species and outward of the 6f-Ti and 3f-O, therefore making the final structure more puckered.

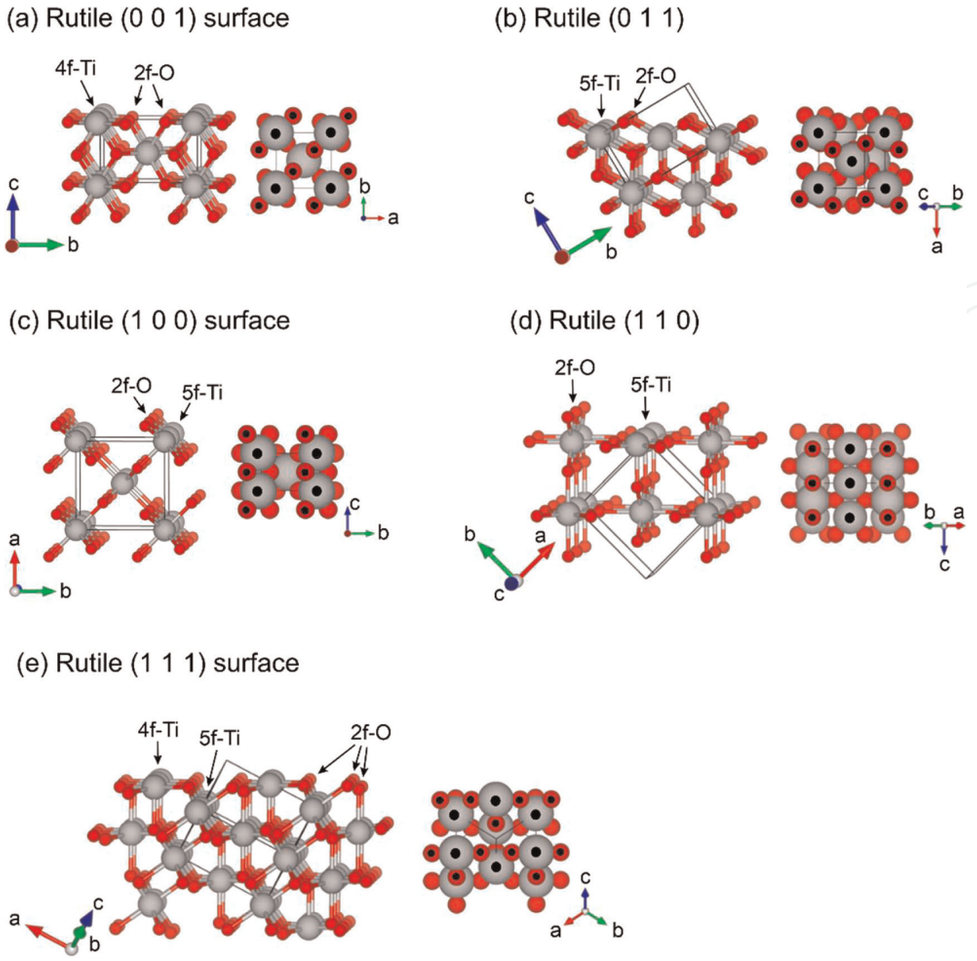

Figure 2.
Perfect, bulk-cut atomic geometries of different rutile surfaces. Figure features are analogical to the anatase one.

Finally, the rutile (1 1 1) surface is rarely discussed; however, a detailed analysis of its possible structure was presented by Wang et al. [18]. For the unreconstructed, bulk-cut, stoichiometric surface, the corresponding surface energy was found to be in the range of 1.34 $J \cdot m^{-2}$, exposing ⅓ of Ti atoms as 4f-Ti in the first layer, ⅓ of Ti as 5f-Ti in the second one, and hypothetically ⅓ of 6f-Ti in the third one. Here, all O atoms in the first layers are 2f-coordinated and 3f-O can be found only below the 5f-Ti sites, as shown in **Figure 2e**. According to Jiang et al., the 4f-Ti atoms show significant inward relaxation for such a structure [13]. However, very high surface energy and density of undercoordinated atoms generally lead to the instability of such "perfect" (1 1 1) surface, and further stabilization by hydroxylation was discussed in the following parts.

2.3 Unreconstructed brookite surfaces

Finally, **Figure 3** shows unreconstructed brookite surfaces, which are analogical to the anatase and rutile. Compared to the other polymorphs, brookite surfaces form rather complex structures, often exposing 4f-Ti. Due to such complexity, the calculated fraction of undercoordinated species for brookite surfaces is presented only for Ti atoms. Moreover, in the case of most surfaces, multiple terminations can be considered. Here, we have highlighted only those, which were found to be most stable, or whose reconstructed geometries showed significant stabilization.

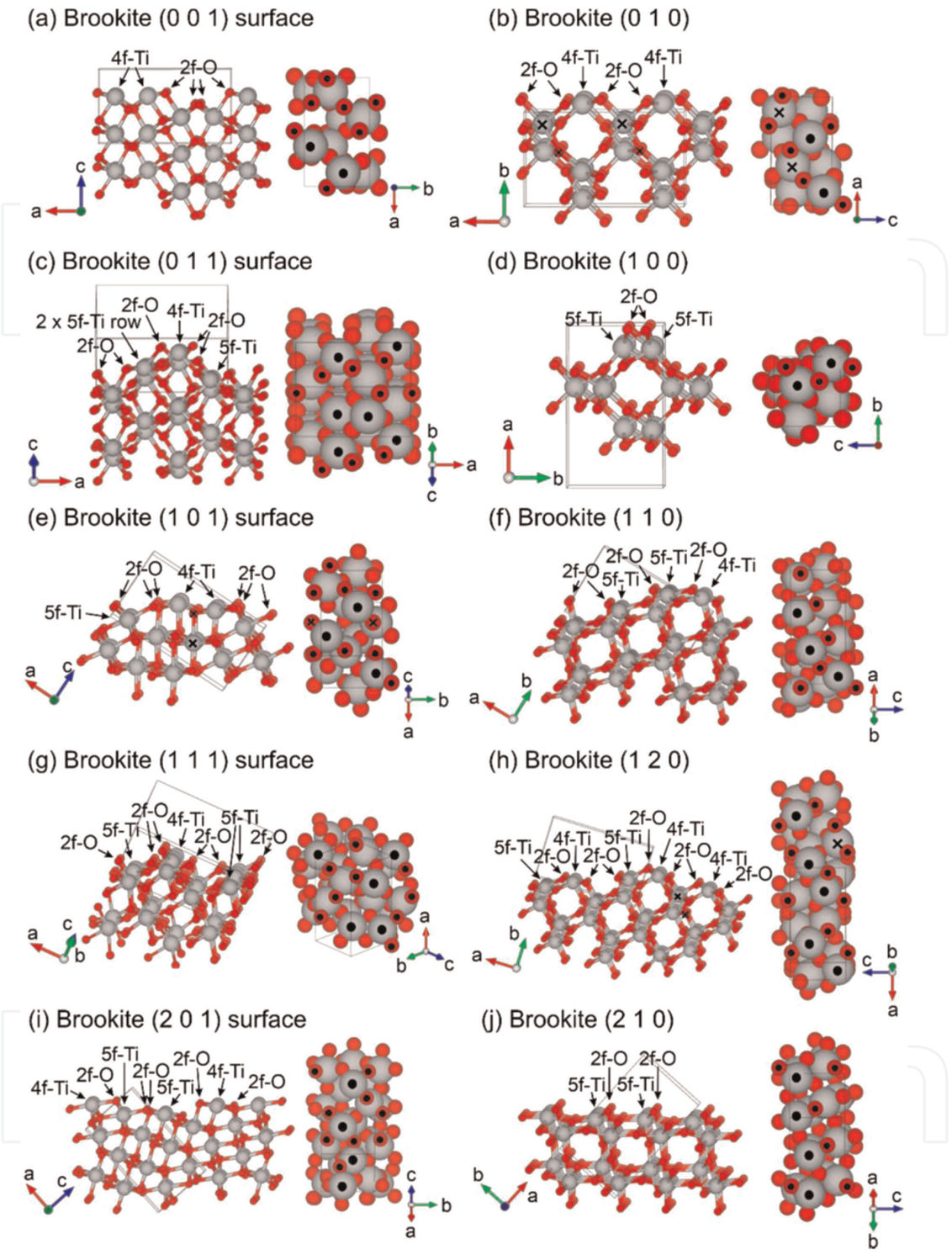

Figure 3.
Perfect, bulk-cut atomic geometries of different brookite surfaces. Figure features are analogical to the anatase one. The "X" mark indicates possible bond breaking after relaxation.

The (0 0 1) brookite surface directly exposes 4f-Ti and 6f-Ti; however, some additional 6f-Ti, that are partially exposed can be found in the deeper parts of the surface, as presented in **Figure 3a** (after including deeper-layer Ti fraction of 4f-Ti is ¼). The top Ti atoms are bridged with a network of 2f-O and saturated O can be found only in the deeper parts of the surface. The calculated energy of such geometry after

straightforward optimization was found to be 1.18 $J \cdot m^{-2}$; however, possible reconstruction is known to stabilize alternate geometry, which will be discussed later.

Furthermore, the (0 1 0) brookite surface shows structure similar to the anatase (1 1 0) and rutile (0 0 1), with a top layer of (2f-O)-(4f-Ti)-(2f-O) bonding to the 6f-Ti in cavities. Assuming exposition up to the first three Ti layers, the fraction of 4f-Ti is ¼ for such geometry. Moreover, reported relaxation has shown that the uppermost 6f-Ti significantly rises to the top, breaking one bond with a deeper layer 3f-O, as highlighted with "X" in **Figure 3b**. Therefore, additional 5f-Ti is expected to be exposed on the relaxed surface. The final surface energy of such a structure was found to be 0.77 $J \cdot m^{-2}$. Focusing on the next structure, the (0 1 1) brookite surface is shown in **Figure 3c**, exposing a combination of both 4f-Ti (⅛), 5f-Ti (⅜), and 6f-Ti (½), which are connected by a quite complex network of both undercoordinated and fully coordinated O atoms. Relaxation of the structure leads to outward displacement of 6f-Ti, while undercoordinated titanium relaxes inward the crystal structure, giving final surface energy of 0.74 $J \cdot m^{-2}$. The (1 0 0) brookite surface is similar to the anatase (1 1 2), with a sawtooth-like profile, as shown in **Figure 3d**. The top of the surface directly exposes a row of 5f-Ti (½) atoms connected by the 2f-O, while deeper layers are fully coordinated. It can be noted that this structure can possess two very similar, but not strictly identical, configurations, where the top of the surface is composed of either the first or the second Ti layer, as shown in **Figure 3d**. Gong and Selloni [15] reported that these two configurations differ slightly in surface energy (either 0.88 or 0.93 $J \cdot m^{-2}$). Nevertheless, their overall geometry is very similar, and both configurations differ mostly due to slight changes in the exact bond lengths and angles at the very top. Next, **Figure 3e** shows the structure of the perfect (1 0 1) brookite surface, again exposing a combination of 4f-Ti (¼), 5f-Ti (⅛), and 6f-Ti (⅝), connected with both saturated and 2f-coordinated O atoms. Significant changes in the perfect structure during the relaxation include bond breaking between 3f-O that bridges two surface 4f-Ti atoms and the subsurface 6f-Ti, highlighted in **Figure 3e** with "X." In this case, the resulting 5f-Ti is located in the subsurface region; however, additional 2f-O appears exposed directly on the surface top. The resulting surface energy for such geometry is 0.87 $J \cdot m^{-2}$. The surface structure of brookite (1 1 0) presented in **Figure 3f** is characterized by terraces that end with a 4f-Ti edge and further step-down. Again a variety of Ti species are exposed at this surface ($^1/_7$ of 4f-Ti and $^2/_7$ of 5f-Ti). Undercoordinated atoms undergo large relaxation at the edges, with O atoms relaxing outward the crystal structure and Ti atoms relaxing inward. The corresponding surface energy was found to be 0.85 $J \cdot m^{-2}$. The (1 1 1) surface of brookite can be considered in a variety of different, complex terminations, which were studied in detail by Gong and Selloni. Following their results, **Figure 3g** shows the most probable (1 1 1) structure, exposing ⅛ of Ti sites as 4-fold coordinated and ⅜ as 5f-Ti. No significant relaxation changes were reported for such a structure and the corresponding surface energy was 0.72 $J \cdot m^{-2}$. Next, the (1 2 0) brookite surface is shown in **Figure 3h**, exposing 4f-Ti ($^3/_{13}$) and 5f-Ti ($^2/_{13}$). This is another brookite surface that shows possible bond breaking between saturated Ti and O after the relaxation, as indicated in the surface model with "X," which results in the appearance of the additional 5f-Ti site at the surface's top. The corresponding surface energy was 0.82 $J \cdot m^{-2}$. Furthermore, the (2 0 1) brookite surface was not investigated in detail through a computational approach; however, it has gained significant experimental attention due to reported relatively high photocatalytic activity. The atomic model of the (2 0 1) surface, proposed by Lin et al., and Zhou et al., is shown in **Figure 3i** [16, 19]. This surface composes of little up-and-down terraces, exposing either 4f-Ti

($^2/_7$) or 5f-Ti ($^2/_7$), respectively. On the "flat" parts, the two 5f-Ti are bridged with two 2f-O, while two 4f-Ti are bridged with one 2f-O and one 3f-O. Additional 2f-O are present at the edge of each step. Finally, **Figure 3j** shows the energetically most stable brookite surface (2 1 0), with reported surface energy of 0.70 $J \cdot m^{-2}$. The atomic geometry of this surface shows similarities with anatase (1 0 1), as both expose characteristic steps of undercoordinated 5f-Ti bonded to the 2f-O at the edge of the step. Lower parts of the surface, below the (5f-Ti)-(2f-O) steps, are fully coordinated. The final fraction of 5f-Ti for this surface is ½. Similar to other TiO_2 surfaces, the 6f-Ti and topmost 3f-O show visible relaxation outward of the crystal structure, while 5f-Ti relax inward.

2.4 Surface energies and reconstructions

The above description shows possible terminations of the TiO_2 crystals by different crystal planes, resulting in different surface energies calculated for relaxed models. Concerning analyses in a vacuum, these energies roughly correspond to the density of theoretical bonds that needs to be broken to form particular termination. However, as presented in **Figure 4**, considering different values reported in the literature, the relationship is not always strict and should be considered more as a guidance than an actual rule. It should also be noted that different computational details will lead to different computed energy values, which should be especially minded.

As presented in **Figure 4**, some of the reported energies can achieve quite large values, which is commonly the reason why such hypothetical structures are not necessarily observed experimentally. This may include the fact that analyzed crystals/nanoparticles do not terminate in such orientation or that the final structure does not correspond to such particular atomic geometry. The second option is generally known as surface reconstruction, where interface atoms adopt geometry different from the corresponding crystal plane to minimize final surface energy.

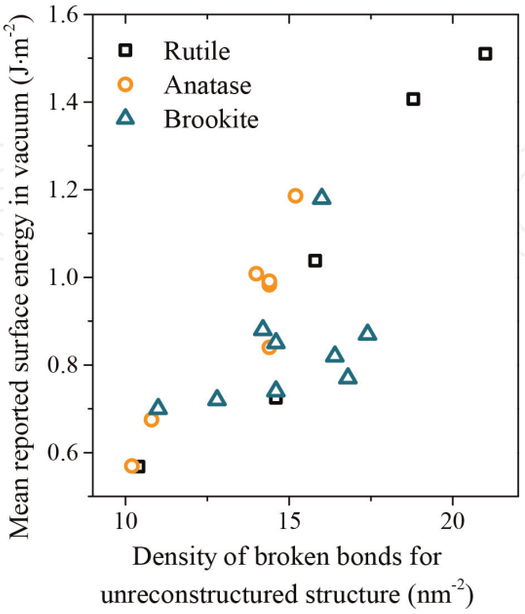

Figure 4.
Relation between reported surface energies of different, unreconstructed TiO2 surfaces in vacuum and a density of broken bonds, needed to form the surface from bulk crystal. To give better comparison between values obtained in different studies (no single study reports all considered surfaces), final values are presented as a mean.

Surface reconstruction was reported as an important process for several possible TiO_2 terminations. Probably, the most notable is the (1 x 4) reconstruction of the anatase (0 0 1) surface, which was described in the early 2000s and should be especially considered under ultra-high vacuum conditions [20–22]. The probable structure of such termination was proposed by Lazzeri and Selloni with the "admolecule" model, which was found to be energetically more stable than the unreconstructed surface (0.51 $J \cdot m^{-2}$ for the reconstructed geometry, vs. 0.90 $J \cdot m^{-2}$ for the unreconstructed one) [8]. In their model, they propose that every fourth of the (5f-Ti)-(2f-O)-(5f-Ti) periodic units, shown in **Figure 1a**, is replaced by the row of TiO_3 bridging species that rise above the perfect surface. The stability of such a configuration was explained due to the stress relief induced by the change in the bond length between the 5f-Ti and 2f-O atoms "left" in the unreconstructed part of the surface. Specifically, the (1 x 4) periodicity of such reconstruction resulted in the bond length being the closest to the "natural" length and, in consequence, the lowest surface energy. Nevertheless, despite the energetical stability of the proposed model, such a structure was not found to be completely in agreement with the experiment. This was mostly due to the relatively low activity of such structures, despite the expected exposition of the 4f-Ti atoms at the formed bridges, which should act as good adsorption and dissociation centers. This has led to further refinement of the proposed geometry by Wang et al. where they suggested that exposed 4f-Ti became oxidized to the fully-coordinated 6f-Ti [23]. The atomic geometry of their model is shown in **Figure 5**, where 5a and 5b correspond to the non-defected surface, while other images show different defect sites observed during the scanning tunneling microscopy (STM) analysis. In conclusion, they have shown that oxidized reconstruction is chemically inert and only reduced 4f-Ti sites show considerable activity.

However, despite a lot of attention being given to such (1 x 4) reconstruction, the actual geometry of the anatase (0 0 1) surface during growth and in aqueous suspensions is still probable to be unreconstructed. This fact is firstly justified by the fluorine stabilization of the (0 0 1) surface in its unreconstructed form, which is commonly used during the preparation procedure of such nanocrystals (details of this stabilization are described in the following section). After such preparation, fluorine has to be removed from the surface, as well an energy barrier needs to be overcome to induce the reconstruction. Both of these processes are known to occur in temperatures above 500–600°C, and below this temperature, reconstruction is not obvious [24–26]. Moreover, the possible stability of the unreconstructed geometry was experimentally confirmed by DeBenedetti et al. in the aqueous carboxylic acid solution [27]. Therefore, although (1 x 4) reconstruction of the anatase (0 0 1) surface should be minded, the actual geometry should be carefully considered, depending on the experimental details and available techniques.

Furthermore, different reconstructions were also proposed for other TiO_2 surfaces, and their general summation is presented in **Table 1**. Noticeably, a variety of rutile surfaces are expected to reconstruct, including (0 0 1), (0 1 1), and (1 0 0) terminations. Interestingly, these surfaces are also expected to be present in the equilibrium shape of the rutile crystal, as shown later. The (0 0 1) rutile surface is generally known to reconstruct or facet, especially in higher temperatures [28–30]. Commonly, the {0 1 1} and {1 1 4} facets are reported to form at the (0 0 1) surface, from which the {0 1 1} facets are also expected to adopt the geometry of the (2 x 1) reconstruction of the (0 1 1) surface itself. Detailed studies of this (2 x 1) reconstruction were presented by several authors, generally proposing a "brookite (0 0 1)-like" atomic structure [31–33]. This structure shows a characteristic topmost zigzag, composed of

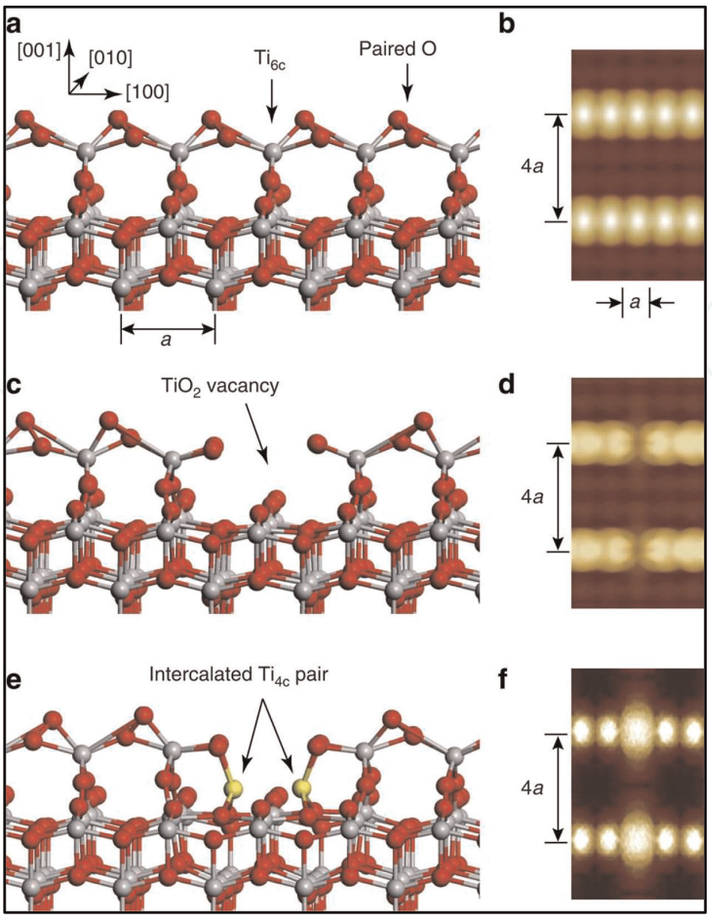

Figure 5.
Atomic models of the anatase (0 0 1) surface after the oxidized (1 x 4) reconstruction proposed by Wang et al. [23]. Non-defected (a) and defected (c, e) structures. Panels (b, d, and f) show corresponding simulated scanning tunneling microscope images. Please note that models (a, c, and e) are shown in parallel to the (1 x 4) periodicity of the reconstruction. Reprinted from [23] under a creative commons attribution 3.0 Unported license.

Polymorph and surface	Periodicity	Geometry	Specific formation conditions
Anatase (0 0 1)	(1 × 4)	Row of 6f-coordinated Ti above the bulk-like surface.	Ultra-high vacuum and annealing in 500–600°C.
Rutile (0 0 1)	Not discussed	{0 1 1} and {1 1 4} microfacets.	Annealing in 750–780°C.
Rutile (0 1 1)	(2 × 1)	Brookite (0 0 1)-like.	Not discussed.
Rutile (1 0 0)	(1 × 3), (1 × 5), (1 x 7)	{1 1 0} microfacets, partially reduced.	Annealing in the ultra-high vacuum.
Brookite (0 0 1)	(1 × 1)	Several bonds breaking between surface and subsurface species, topmost exposition of the 2f-O.	Not discussed.

Table 1.
Summation of the most important reported reconstructions of the TiO2 surfaces.

the 5f-Ti and 2f-O, observed in the STM images. As reported by Gong et al., surface energy of such a configuration was found to be 0.42 $J{\cdot}m^{-2}$, while the unreconstructed surface of about 0.89 $J{\cdot}m^{-2}$ is under the same computational parameters [33]. Furthermore, the (1 0 0) rutile surface can especially reconstruct after annealing in the

ultra-high vacuum conditions, showing the formation of the {1 1 0} microfacets with several reconstruction patterns, such as a (1 x 3), (1 x 5), and (1 x 7). Commonly, the (1 x 3) reconstruction is considered, which was recently studied by Balzaretti et al. concerning its surface energy and interactions with water [34]. Interestingly, they observed that reconstructed geometry is slightly less stable (0.04 $J \cdot m^{-2}$ difference) than unreconstructed one. It is also noteworthy that photoemission experiments have shown that such annealed, reconstructed surface is partially reduced, which might influence its stability [29]. Finally, reports about brookite surfaces are relatively rare. Therefore, possible reconstructions of its geometries are also not discussed. Nevertheless, Gong and Selloni reported an important reconstruction of the (0 0 1) surface, which results in a reduction of its surface energy from 1.18 to 0.62 $J \cdot m^{-2}$, making it one of the most exposed surfaces in the equilibrium shape [15]. This structure is very similar to the proposed (2 x 1) reconstruction of the rutile (0 1 1) surface. In this reconstruction, the 3f-O atoms, that were originally bridging the 4f-Ti atoms (see **Figure 2a**), break their bonds with subsurface 6f-Ti and rise above the 4f-Ti. Simultaneously, two subsurface 3f-O break their bonds with surface 6f-Ti and move toward each other, ultimately locating below the 4f-Ti pair.

3. Facets stabilization, crystal shapes, and synthesis strategies

According to general thermodynamics, the total surface energy of the crystal should be minimized for the whole system to achieve minimum energy. Therefore, the exposition of some crystal planes is not expected. However, to consider such a lowest-energy shape, it is first necessary to consider the formation of surfaces equivalent to the specific model. For example, for the anatase polymorph, the (1 0 0), ($\bar{1}$ 0 0), (0 1 0), and (0 $\bar{1}$ 0) have the same atomic arrangement and are equivalent. Therefore, if the (1 0 0) surface became stable at the considered conditions, it is expected that four analogical facets will form in the crystal, with their orientation being the same as the orientation between the crystal planes. The family of such equivalent crystal planes is denoted using brackets and their Miller indices, which are also used to index observed crystal facets. The most important TiO_2 facets and their corresponding equivalent crystal planes are listed in **Table 2**.

Finally, after considering possible surface terminations, their energies, and equivalent planes, the 3-dimensional minimum-energy crystal shape can be obtained, according to the Gibbs-Curie-Wulff theorem [35]. This shape is also called the Wulff construction. Concerning the anatase, rutile, and brookite, their corresponding Wulff constructions are shown in **Figure 6**, according to the existing studies [5, 14, 15].

Constructions shown in **Figure 6** can be seen as a perfect case, and therefore, it is not unusual that experimentally obtained micro- or nanostructures can exhibit a variety of very different shapes. This results from two important aspects of the preparation procedure. Firstly, the adsorption of a different species can drastically change the energy of a final surface. Moreover, and more importantly, the relative energy of different surfaces might also change, leading to a situation where minimum-energy construction will expose a completely new set of different facets. Such energetic stabilization is often achieved by the addition of specific capping agents, pH control, or growing on a substrate. The second aspect is the kinetics of such growth. Particularly, very fast nucleation of the substrate can lead to the situation where final nanoparticles will not form a well-defined geometry, despite a thermodynamic preference to grow in some specific direction. In the case of TiO_2, this can typically be

Polymorph	Facet {*h k l*}	No. of equivalent crystal planes	Crystal planes
Anatase	{0 0 1}	2	(0 0 1), (0 0 $\bar{1}$)
	{1 0 0}	4	(1 0 0), ($\bar{1}$ 0 0), (0 1 0), (0 $\bar{1}$ 0)
	{1 0 *l*}	8	(1 0 *l*), (0 1 *l*), ($\bar{1}$ 0 *l*), (0 $\bar{1}$ *l*), (1 0 $\bar{l}$), (0 1 $\bar{l}$), ($\bar{1}$ 0 $\bar{l}$), (0 $\bar{1}$ $\bar{l}$)
	{1 1 0}	4	(1 1 0), ($\bar{1}$ 1 0), (1 $\bar{1}$ 0), ($\bar{1}\bar{1}$ 0)
Rutile	{0 0 1}	2	(0 0 1), (0 0 $\bar{1}$)
	{0 1 1}	8	(0 1 1), (1 0 1), (0 $\bar{1}$ 1), ($\bar{1}$ 0 1), (0 1 $\bar{1}$), (1 0 $\bar{1}$), (0 $\bar{1}$ $\bar{1}$), ($\bar{1}$ 0 $\bar{1}$)
	{1 0 0}	4	(1 0 0), ($\bar{1}$ 0 0), (0 1 0), (0 $\bar{1}$ 0)
	{1 1 0}	4	(1 1 0), ($\bar{1}$ 1 0), (1 $\bar{1}$ 0), ($\bar{1}\bar{1}$ 0)
	{1 1 1}	8	(1 1 1), (1 $\bar{1}$ 1), ($\bar{1}$ 1 1), ($\bar{1}$ $\bar{1}$ 1), (1 1 $\bar{1}$), (1 $\bar{1}$ $\bar{1}$), ($\bar{1}$ 1 $\bar{1}$), ($\bar{1}$ $\bar{1}$ $\bar{1}$)
Brookite	{*h* 0 0}, {0 *k* 0}, {0 0 *l*}	2	Combination of all possible $\bar{h}$, $\bar{k}$, and $\bar{l}$
	{*h k* 0}, {*h* 0 *l*}, {0 *k l*}	4	
	{*h k l*}	8	

Table 2.
Summation of the most important TiO2 facets and their corresponding crystal planes.

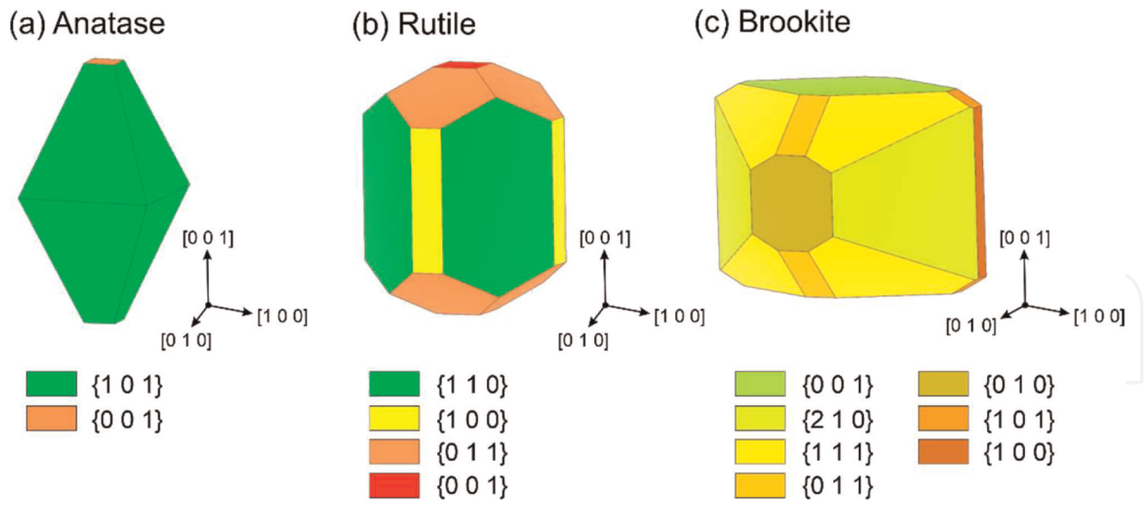

Figure 6.
Wulff constructions of the (a) anatase, (b) rutile, and (c) brookite TiO2 crystals, based on the existing studies [5, 14, 15]. Adapted colors generally follow the reported surface energy.

addressed using "dissolution-recrystallization" processes, where nucleated seeds are dynamically dissolved and then recrystallized in the rebuilt, stable crystal shape [36]. Alternatively, Ti-precursors, which will nucleate slower, can be used to achieve more stable growth. For example, when using Ti-alkoxides as precursors, it is known that a longer carbon chain should result in slower nucleation [37]. Ultimately, both kinetic and thermodynamic aspects should be considered when designing a synthesis route

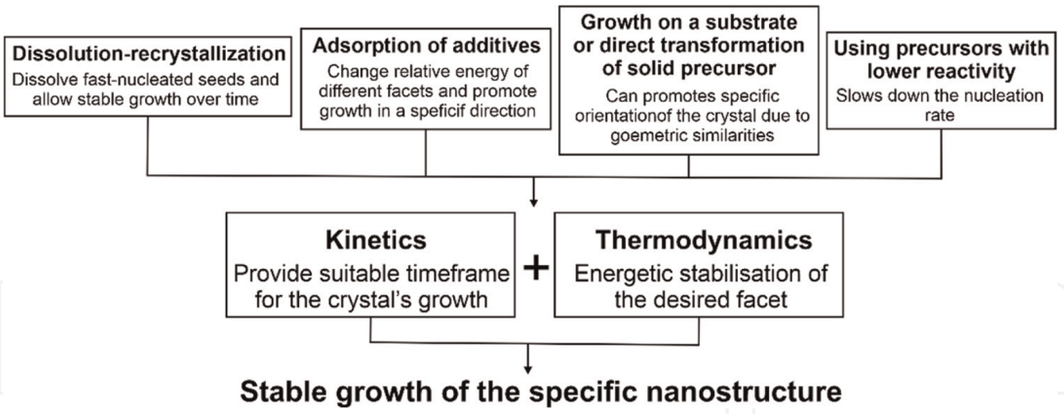

Figure 7.
Summation of the most important aspects and some strategies used for the preparation of faceted TiO2 nanostructures.

for a specific facet exposition. It is also noteworthy that multiple effects can be ascribed to the same additive. For example, during the HF-assisted growth of anatase nanostructures, hydrofluoric acid enables both dissolution of the TiO_2 nuclei and thermodynamically stabilized {0 0 1} facets [26]. A summation of general synthesis strategies is presented in **Figure 7**.

The hydrothermal process is usually used under specific synthesis conditions to obtain desired crystal shapes, considering the appropriate precursor, capping agent, and solvent. Various reaction substrates or ions can play a role as a capping agent in the synthesis. Therefore, in the next subsections, the most important synthesis strategies are described, together with highlighting the key factors.

3.1 Anatase crystal facets and shapes

The evolution of the anatase crystal shapes due to the exposition of different crystal facets is shown in **Figure 8**. Although the formation of a range of different facets was reported, the most investigated anatase crystal facets in the literature are {1 0 1}, {1 0 0}, and {0 0 1}, from which the first two facets are low energetic. Due to the symmetry of anatase crystal structure, nanocrystals with exposed {1 0 1} facets are octahedral, whereas the {0 0 1} facets form anatase nanosheets. Moreover, the combination of {1 0 1} and {0 0 1} facets (decahedral anatase nanostructures) and {0 0 1} and {1 0 0} (anatase cuboids) are also extensively studied. Decahedral nanocrystals may also undergo further flattening to nanosheets, resulting in dominant {0 0 1} facets. As reported by Barnard and Curtiss, the relative stability of these three facets depends heavily on the hydrogenation/oxygenation of the surface and, therefore, is strongly affected by the pH of the solution [11]. One of the consequences is that {1 0 1} and {1 0 0} exposing structures can be prepared in similar conditions, but {1 0 0} requires a higher pH. Alternatively, due to our best knowledge, the formation of the {0 0 1} exposing structures in the basic pH was not yet reported.

Anatase with exposed {1 0 1} facets is characterized by the lowest surface energy. Alone they form octahedral nanostructures, which synthesis methods are presented in **Table 3**. The most described procedure is a two-step synthesis, in which the first step is the fabrication of potassium titanate nanowires from a hydrothermal reaction of TiO_2 P25 (or other commercial TiO_2) in KOH solution. The second step is not always the same. For example, Amano et al. proposed direct hydrothermal treatment of titanate

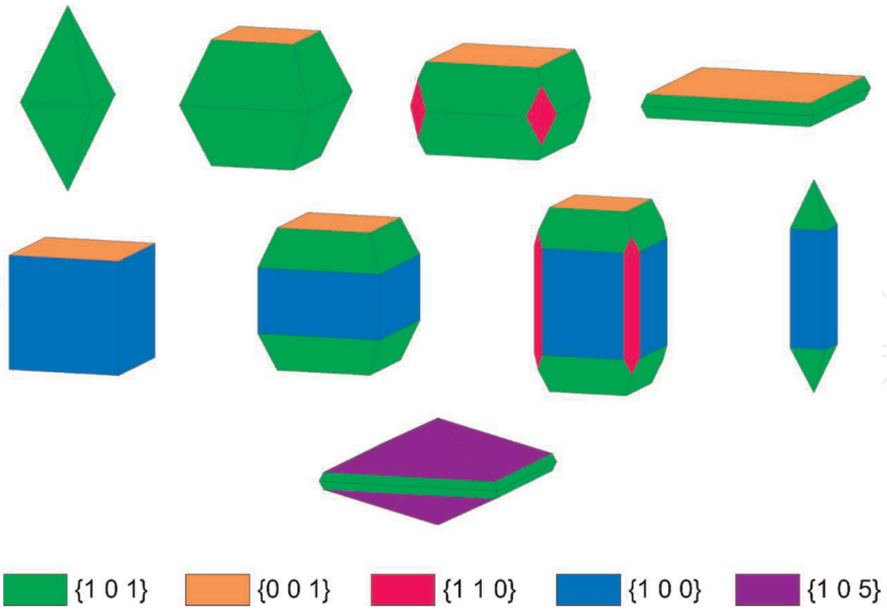

Figure 8.
The possible anatase crystal shapes resulting from the exposition of different crystal facets.

Precursor	Synthesis route and conditions	Comments	Ref.
Potassium titanate nanowires	Hydrothermal; 170°C, 24 hours	The proportion of regular octahedral bipyramids was ca. 70%	[38]
Potassium titanate nanowires, NH_4NO_3, HMTA	Hydrothermal; 200°C, 24 hours	Relative high yield of regular octahedral bipyramids >80%	[39]
$TiCl_4$, oleylamine	Synthesis in Schlenkline; quickly heating at 290°C	—	[40]
$TiOF_2$, hydrazine	Hydrothermal; 210°C, 24 hours	—	[41]
$Ti(SO_4)_2$, hydrazine	Hydrothermal; 200°C, 12 hours	The productivity of anatase octahedra was over 80%	[42]

Table 3.
Selected synthesis of octahedral anatase nanocrystals with exposed {1 0 1} facets.

nanowires. This synthesis resulted in the formation of mesoparticles with exposed {1 0 1} facets. The proportion of regular octahedral bipyramids in the nanostructures was about 70% [38]. A different route is the production of ammonium-exchanged titanate nanowires from $K_2Ti_6O_{13}$ precipitates obtained during the first step [39]. The above description considers mainly octahedral anatase nanostructures with the exposed {1 0 1} facets. However, according to Wang et al., these bipyramidal facets were obtained under hydrothermal conditions using potassium titanate nanowires as a precursor, hydrogen peroxide, and hydrofluoric acid as capping agents [43]. Alternatively, hydrazine-assisted formation of the {1 0 1} octahedrons was reported when starting from the precursors like $TiOF_2$ and $Ti(SO_4)_2$ [41, 42].

Another low-energetic anatase crystal facet is {1 0 0}, which synthesis methods are presented in **Table 4**. This crystal facet usually co-exists with other crystal facets and forms cuboids or rectangular prisms with truncated prisms [40, 41]. However, some

Precursor	Synthesis route and conditions	{1 0 0} facets exposition (%)	Comments	Ref.
$TiCl_4$, HCl, $NaBF_4$	Hydrothermal; 130°C, 12 hours	45	55% {0 0 1}	[44]
TiF_4, ethanol, oleic acid	Solvothermal; 200°C, 40 minutes	95	Anatase Nanosheets	[45]
Na-titanate	Hydrothermal; 120°C, 24 hours	Not mentioned	Nanorods	[46]
$TiOF_2$, NH_3	Hydrothermal; 210°C, 24 hours	Not mentioned	Co-exist with {1 0 1} and {0 0 1}	[41]

Table 4.
Selected synthesis of anatase nanocrystals with exposed {1 0 0} facets.

syntheses with a high percentage of {1 0 0} crystal were also successfully performed. For example, Xu et al. reported the preparation of anatase nanosheets with exposed {1 0 0} facets [44]. Previously, nanosheets and nanocrystals were combined with {0 0 1} facets exposition. The second possible shape of nanostructures is nanorod, which synthesis was described by Li and Xu. The precursor was sodium titanate obtained from a facile hydrothermal route during the reaction of P25 in sodium hydroxide solution. Anatase nanorods with {1 0 0} facets were transformed from Na-titanate *via* exchanging alkali-ions with protons under alkaline conditions to form the H-titanates [45].

The starting point for the investigation on the high-energetic anatase crystal facets was the research of Yang et al. [26], who proved that {0 0 1} facets could be energetically preferable to {1 0 1}, although the surface energy of {0 0 1} facets is, in general, higher than {1 0 1}. The main requirement was the addition of fluorine to the reaction environment. In these theoretical studies, among the surface termination using 12 elements (H, B, C, N, O, F, Si, P, S, Cl, Br, or I), only fluorine-terminated surface allowed to stabilize {0 0 1} facets rather than {1 0 1}. These calculations were completed by experiments in which anatase nanostructures with exposed {0 0 1} facets were successfully synthesized using the hydrothermal approach with hydrofluoric acid as a capping agent. However, in the above experiments, {0 0 1} facets accounted for only ~47% of all exposed crystal facets. In the meantime, Wen et al. [46] showed the synthesis of anatase nanocrystals with exposed {0 0 1} facets using 1-butanol as a solvent. This procedure allowed obtaining of large-sized well-defined anatase nanosheets wholly dominated with {0 0 1} and {1 0 0} facets, which had a percentage of 98.7% and 1.3%, respectively. The results can be explained by the alcohol stabilization effect associated with fluorine adsorption over the (0 0 1) surface. The role of particular alcohols, especially aliphatic with different chain lengths, was systematically studied recently [37, 47, 48].

The comparison of the anatase nanosheets with exposed {0 0 1} facets is presented in **Table 5**. In most studies concerning TiO_2 with exposed {0 0 1} facets, hydrofluoric acid was used in the experimental procedure. However, other fluoride-based reagents were also investigated. For example, ionic liquids (IL) were applied for stabilization of these high-energetic facets, e.g., 1-butyl-3-methylimidazolium hydrogen sulfate [Bmim]HSO_4 and 3-methyl-1-(3-sulfonyl propyl) imidazolium trifluoro methane sulfonate [$HO_3S(CH_2)_3MIM$][CF_3SO_3] [18]. Moreover, the fluorine atoms can be delivered by using an appropriate Ti source. An example of the compound in the Ti-O-F

Precursor and F source	Synthesis route and conditions	{0 0 1} facets exposition (%)	Comments	Ref.
TiF_4, HF, 1-butanol	Solvothermal; 210°C, 24 hours	98.7	Large size in length (ca. 4.14 μm).	[47]
TBT, HF	Hydrothermal; 250°C, 24 hours	75	—	[49]
TBT, HF, isobutyl alcohol	Solvothermal; 180–200°C, 20 hours	97	Flower-like structure with ca. 2.0 mm	[50]
Degussa P25, HF, H_2O_2	Hydrothermal; 180°C, 10 hours	65	Truncated bipyramidal anatase	[51]
$TiOF_2$	Calcination at 300–900°C, 2 hours	>83	—	[52]
TiF_4, diethylene glycol, acetic acid	Solvothermal; 180°C, 8 hours	>90	—	[53]
$HFTiO_3$, HF	Vapor-phase hydrothermal; 230°C, 3 hours	98.2	—	[54]
TiF_4, $[bmin]^+$ $[BF4]^-$	Microwave-assisted; 210°C, 1.5 hours	80	—	[55]
TiF_4, 1-Methylimidazolium tetrafluoroborate	Microwave-assisted; 210°C, 1.5 hours	50	—	[56]
$TiCl_4$, ethylene glycol	Solvothermal; 240°C, 48 hours	55	Hexagonal nanoplatelets	[57]

Table 5.
Selected synthesis of anatase nanocrystals with exposed {0 0 1} facets.

system is titanium oxyfluoride ($TiOF_2$), which can transform to TiO_2 *via* a solvothermal process [36] or simple calcination at a temperature above 600°C [58].

Moreover, next to {0 0 1} and {1 0 1} facets, a small rhombus originating from {1 1 0} facet exposition with a surface energy of about 1.09 $J \cdot m^{-2}$ can be formed. Liu et al. reported that the hydrothermal treatment of metallic Ti powder together with the combination of hydrofluoric acid and hydrogen peroxide allowed the formation of these highly energetic facets. It was described that HF was responsible for Ti dissolution, whereas H_2O_2 reacted with Ti^{4+} to obtain peroxotitanium acid. This complex slows down the hydrolysis rate, which is necessary to pack the Ti–O–Ti chains and finally form {1 1 0} facets [59]. Similar results were obtained by Li et al., who used $TiCl_3$ instead of Ti powder for the fabrication of {1 1 0} facets of anatase [49].

Excluding {1 1 0} facets, other synthesis procedures of anatase crystals with exposed high-index facets have been reported in the literature. For example, Xu et al. reported the synthesis of anatase single crystals with the exposed {1 1 1} facets. According to the density functional theory calculations, their surface energy was 1.61 $J \cdot m^{-2}$, which was explained by a high percentage of undercoordinated Ti and O atoms on the (1 1 1) surface [50]. Finally, Jiang et al. performed a gas-phase oxidation process using $TiCl_4$ as a precursor, which led to obtaining anatase single crystals with exposed high-index {1 0 5} facets. The regulation of the Ti/O ratio in the reaction system enabled inhibition of the growth of other crystal facets like {1 0 1} or {1 0 3}

[17]. Therefore, the research direction to obtain high-index crystal facets with relatively high surface energy is still under further investigation. However, there is a probability that non-equilibrium conditions and sophisticated synthesis will be necessary to preserve this surface.

3.2 Rutile and brookite crystal facets and shapes

Compared to anatase, preparation procedures of both rutile and brookite polymorphs are far less investigated. Moreover, observed nanocrystals are commonly not consistent with a theoretical Wulff construction. In the case of rutile, above all, this is due to the commonly observed appearance of the {1 1 1} facets after the hydrothermal processes. As discussed previously, the (1 1 1) surface in its bulk-terminated form is very energetic, and its stabilization can be achieved only through hydroxylation, as reported by Wang et al. [18]. Interestingly, their calculations suggested that after the hydroxylation, the surface energy of the {1 1 1} facets can be similar or even lower than the most stable {1 1 0}. Ultimately, commonly prepared nanocrystals expose a combination of these two facets [51, 52]. However, some authors report even 100% of the {1 1 1} exposition. For example, Wu et al. reported that wholly exposition of the {1 1 1} can be achieved with a suitably high addition of NaF to the reaction solution [53]. Truong et al. synthesized the rutile nanocrystals with unusual {3 3 1} facets [54]. Their preparation route was based on the solvothermal treatment of titanium-glycolate complex in the presence of picolinic acid as an additive. The resulting product possessed a specific aggregated flower-like structure with facets exposed along the (3 3 1) plane. Based on the detailed experimental investigation, it was further proposed that {3 3 1} facets are composed with the periodically repeating {1 1 0} and {1 1 1} microfacets. Other rutile crystals with a less common shape were synthesized by Chen and Lou, who have reported stabilization of the {0 0 1} rutile facets during the hydrothermal growth in the presence of amorphous MoO_3 [55]. The detailed procedure involved the hydrothermal treatment of mixed TiF_4 + HCl and $(NH_4)_6Mo_7O_{24}{\cdot}4H_2O$ + HNO_3 solutions for 5 hours at 180°C. The final product comprised nanosized rutile platelets with {0 0 1} facets exposed aggregated to approximately 500-nm diameter spheres. The summation of the observed rutile crystal shapes is presented in **Figure 9**.

The research on brookite with exposed facets is the most overlooked issue in facet engineering of TiO_2. Three main challenges can be distinguished: firstly, difficulties in obtaining pure brookite phase. Secondly, the pristine brookite is supposed to be

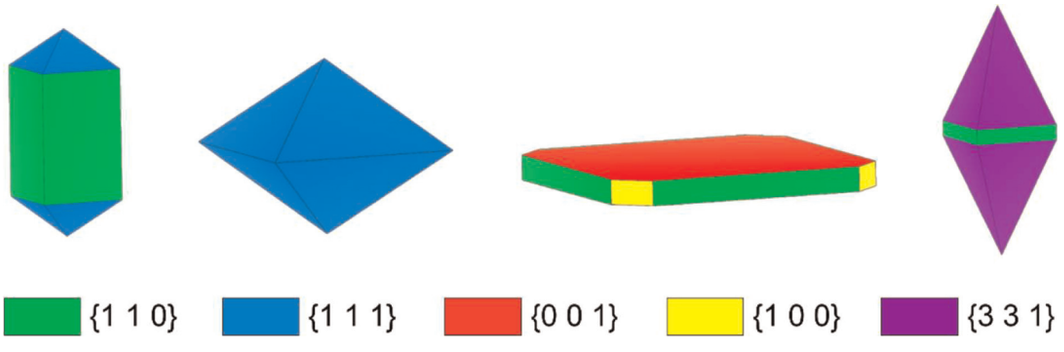

Figure 9.
Scheme of some of the experimentally observed rutile crystal shapes.

photocatalytic inactive. Finally, this TiO_2 polymorph is metastable and undergoes a thermal transition to rutile at high temperatures [56].

However, the rising investigations about brookite in recent years have led to the recognition of this metastable phase as an active photocatalyst. One of the first studies by Lin et al. reported single-crystalline nanosheets surrounded with four {2 1 0}, two {1 0 1}, and two {2 0 1} facets. These nanostructures exhibited higher photocatalytic performance toward methylene orange removal and hydroxyl radical production than commercial TiO_2 P25 [16]. Furthermore, {2 1 0} facets were also predominant in nanocrystals described by Xu et al., who demonstrated a tunable synthesis of brookite nanomaterials with the following shapes: quasi-octahedral, ellipsoid-tipped, and wedge-tipped nanorods [57]. The above results can be explained by the lowest surface energy of (2 1 0) surface among brookite crystals. However, Zhao et al. synthesized and investigated brookite nanostructures with exposed {1 2 1} and {2 1 1} facets. Particularly, TiO_2 with a majority of {1 2 1} facets exposition, which had many undercoordinated atoms on the surface and a lower VB potential, exhibited enhanced photocatalytic activity toward Rhodamine B degradation under simulated solar light. Therefore, the presented examples from the literature proved that crystal facets engineering is a promising approach to obtaining photocatalytic active material from the inactive phase [60].

4. Application in environmental photocatalysis

Following the ongoing demand for sustainable technologies, faceted TiO_2 nanocrystals are primarily studied as possible photocatalysts in various environmental remediation processes. Due to the relatively higher photocatalytic activity, the majority of these studies focus on the anatase polymorph; however, some interesting findings are also reported for rutile and brookite.

Concerning fundamental aspects of reactivity of different facets, it is often desired to compare pristine photocatalysts with the majority of one specific facet exposed. Comparison of their relative activities can give the so-called activity order of the investigated surfaces [61–63]. Initially, it was generally noticed that an increase of the {0 0 1} content on the anatase nanoparticles increases its photocatalytic activity both for water splitting and for degradation of organic pollutants [64–66]. This was straightforwardly connected with the high surface energy of the (0 0 1) surface, which was expected to provide a high density of potentially active sites for the photocatalytic reactions. However, further studies have presented opposite results, leading to a significant reexamination of the problem. For example, studies by Gordon et al. [67], Pan et al. [61], Mino et al. [68], and Mao et al. [63] have shown relatively low photocatalytic activity of the {0 0 1} facets in different reactions. An interesting study was also reported by Günnemann et al., who studied a variety of different TiO_2 surfaces cut from single crystal samples [69]. Their conclusions support observations of relatively lower photocatalytic activity of the anatase {0 0 1} facets, while {1 0 0} were the most active for ·OH generation (using terephthalic acid as a probe) and {1 0 1} showed the highest activity for methanol oxidation. Ultimately, these results showed that, at present, the photocatalytic activity of different crystal facets is hardly connected *a priori* with its surface energy or high density of undercoordinated species, as initially assumed. Instead, possible adsorption, detailed electronic interactions as well as density of charge trapping and transfer are further considered as crucial for the activity of a specific facet. This makes an overall problem very case-specific and due to

our best knowledge, general conclusions are not possible to draw at this moment. Nevertheless, some of the recent details, key factors, and suggested mechanisms can be discussed for specific applications.

4.1 Water treatment from organic pollutants

Concerning photocatalytic degradation of organic pollutants, it is first noteworthy that these studies can be sub-categorized into 3 categories: degradation of dyes, degradation of non-color compounds, and generation of reactive oxygen species (ROS). Particularly, it should be minded that due to possible sensitization, dye degradation can be initiated by a different mechanism than other pollutants, therefore producing possibly different results. In this regard, it is not recommended to use dyes as a model pollutant, when assessing photocatalytic activity toward the degradation of organic compounds in general [70]. Here, we will focus on the reports and mechanisms discussing the degradation of photochemically inactive compounds and the generation of ROS, which is the main issue for current advanced oxidation technologies.

Concerning degradation of persistent pollutants and ROS generation, water, oxygen, and pollutant itself are the main substrates that can react at the photocatalyst surface. Usually, it is assumed that the process is initiated by the photogenerated holes (h^+) that can either oxidize the pollutant, inducing its further transformation, or produce ·OH radicals from H_2O [71, 72]. Simultaneously, excited electrons are often expected to reduce oxygen to the $\cdot O_2^-$, which can also contribute to the final degradation rate; however, their reactivity is much lower than h^+ or ·OH [73]. Based on this description, it could be expected that the photocatalyst with the highest photooxidation ability should achieve the highest degradation rates. Focusing on the anatase, this is in accordance with some of the reported studies showing that the {1 0 0} facets are highly active, especially concerning ·OH generation [45, 69]. This is also in accordance with the simulations performed by Ma et al., who have shown that h^+ localization is the most favored on this facet, compared to the {0 0 1} and {1 0 1} [74]. However, many studies have also reported {1 0 1} facets to be the most photocatalytic active in the degradation process, which cannot be connected to higher h^+ reactivity on this surface. Moreover, our recent studies have shown that {1 0 1} facets revealed higher mineralization efficiency measured as a total organic carbon (TOC) removal during the phenol degradation process, independently of the degradation rate [41]. Interestingly, both of these facts can be attributed to the increased reduction ability of the {1 0 1} facets. First of all, while the reactivity of the $\cdot O_2^-$ is lower than h^+ or ·OH, they are good ring-opening agents, which might promote the efficient conversion of the aromatic compounds to CO_2 [75]. Moreover, possible multi-electron oxygen reduction can also promote the formation of the ·OH, as well as proton transfer from organic compounds to the adsorbed -OH groups, which might initiate the degradation. This problem was specifically investigated in detail for the anatase {1 0 1} facets, which have shown that a combination of O_2 and H_2O on the (1 0 1) surface results in the formation of surface -OH groups [76]. The process was especially favorable in the presence of two excess electrons in the reaction model, therefore connecting it with a possible 2-electron reduction. Importantly, this shows that on the reduced (1 0 1), H_2O can dissociate, forming the final -OH, which is not occurring spontaneously on the perfect surface. These findings have a fundamental meaning for the reactivity of the {1 0 1} facets, especially for water treatment processes, as the -OH groups are a preferable source of the ·OH formation compared to H_2O itself [77]. This is in good agreement with a recent study by Hwang et al., who confirmed that a significant

amount of free ·OH is formed through the oxygen reduction process, based on the $^{18}O_2$ incorporation into the product [78]. Although utilized samples were not strictly faceted during this study, the exposition of the {1 0 1} structures might be expected due to their energetic stability. Furthermore, a recent study by Dudziak et al. showed that a very good correlation could be observed between the activity of the {1 0 1} enclosed anatase samples for degradation of aromatic compounds and higher probability of both h^+ and e^- trapping on these facets, compared to the {0 0 1} and {1 0 0} ones [79]. The combination of these studies suggests a possible mechanism of the {1 0 1} reactivity as the result of e^- induced H_2O dissociation and further generation of ·OH with photogenerated holes. However, more detailed studies might still be needed to clarify it. Finally, recent reports have also shown that the application of nanostructures exposing {1 0 1} facets might result in lower toxicity of the final solution, during the naproxen degradation process, than {0 0 1} ones [80]. Therefore, at this moment, a combination of high reactivity, high TOC removal, and low toxicity makes {1 0 1} a preferable choice for the degradation of organic compounds, especially micropollutants with aromatic structure and high photostability.

Compared to the anatase facets, {1 0 1} in particular, other TiO_2 structures are not studied in detail and generally show markedly lower photoactivity. Nevertheless, a few important findings are worth noticing. First of all, the same reductive pathway of ·OH generation, reported for anatase by Hwang et al., was not observed for rutile, suggesting that especially for the {1 1 0} rutile facets, ·OH generation occurs strictly through H_2O oxidation [78]. Furthermore, the study by Günnemann et al. showed different activities of rutile {0 0 1}, {0 1 1}, and {1 1 1} facets in the methanol oxidation and ·OH generation. Specifically, they reported that {0 1 1} facets exhibited lower methanol oxidation ability, while {1 1 1} generated lower amounts of hydroxyl radicals. Besides, rutile activity in both reactions was fairly similar and generally worse than anatase [69]. Nevertheless, their study did not consider rutile {1 1 0} facets, which on the other hand, were studied by Kobayashi et al. for the oxidation of oxalic acid [52]. In this study, {1 1 0} revealed higher activity than {0 0 1}, which is also in some agreement with the oxidative ·OH generation by this facet. Finally, concerning brookite facets, it is especially worth mentioning that structures co-exposing {2 1 0}, {2 0 1}, and {1 0 1} facets result in significant activity increase for ·OH generation and methyl orange degradation, otherwise not observed for the control brookite samples [16].

4.2 Solar fuel production

In recent years, semiconductor-based materials have been extensively studied for energy applications that can contribute to reducing greenhouse gases. Storing solar energy into the chemical bonds of fuel seems to be a promising way to replace the traditional combustion of fossil fuels with environmentally friendly technology. Specifically, much attention has been paid to photocatalytic H_2 production from water and CO_2 reduction to valuable chemical compounds.

Regarding H_2 generation from water, it should be noted that pristine structures show low activity, and therefore, surface modification with co-catalysts needs to be applied. In the case of the faceted particles, the overall problem deals with specific interactions between the surface and co-catalyst, as well as possible charge separation between different co-exposed facets. Focusing on the single-facet, important findings were reported by Gordon et al., who noticed the higher activity of the anatase modified with Pt for octahedrons exposing {1 0 1} than nanosheets with exposed {0 0 1}

[67]. Similar results were obtained by Wang et al. for anatase nanoparticles modified with Mo_XC as a co-catalyst [81]. This fact is attributed to the increased reduction ability of the (1 0 1) surface, which results in the synergy of TiO_2 and co-catalyst. Recently, specifically, the problem of interactions between (1 0 1) and different possible metal co-catalyst was investigated in detail by Wang and Gong in their computational study [82]. Based on the obtained results, they have proposed alloyed Cu/Pt and Rh/Pt co-catalysts as promising candidates for hydrogen evolution. This concept was based on optimizing the electron transfer between (1 0 1) anatase surface and Cu or Rh as the electron-acceptor and further exposition of Pt as the active part of the co-catalyst. Considered models and their electronic structures are shown in **Figure 10**.

Furthermore, a combination of {1 0 1} with other co-exposed facets can increase the activity of the TiO_2 materials for H_2 generation. For example, Wei et al. presented a detailed comparison between octahedral {1 0 1} and decahedral {1 0 1}/{0 0 1} anatase particles modified with Cu, Ag, and Au nanoparticles. Particularly, a combination of both {1 0 1} and {0 0 1} facets resulted in a slightly higher activity when modified with Ag or Au, as well as a significantly higher activity when modified with Cu [83]. Furthermore, Meng et al. reported increased H_2 production using the decahedral {1 0 1}/{0 0 1} anatase samples, when both facets were selectively modified by Pt and Co_3O_4, respectively [84]. It is especially noteworthy that such a combination of the facet co-exposition and selective modification with optimized co-catalysts was recently proposed to achieve almost 100% of quantum efficiency during water splitting reaction over $SrTiO_3$ photocatalyst [4]. Therefore, it confirms the

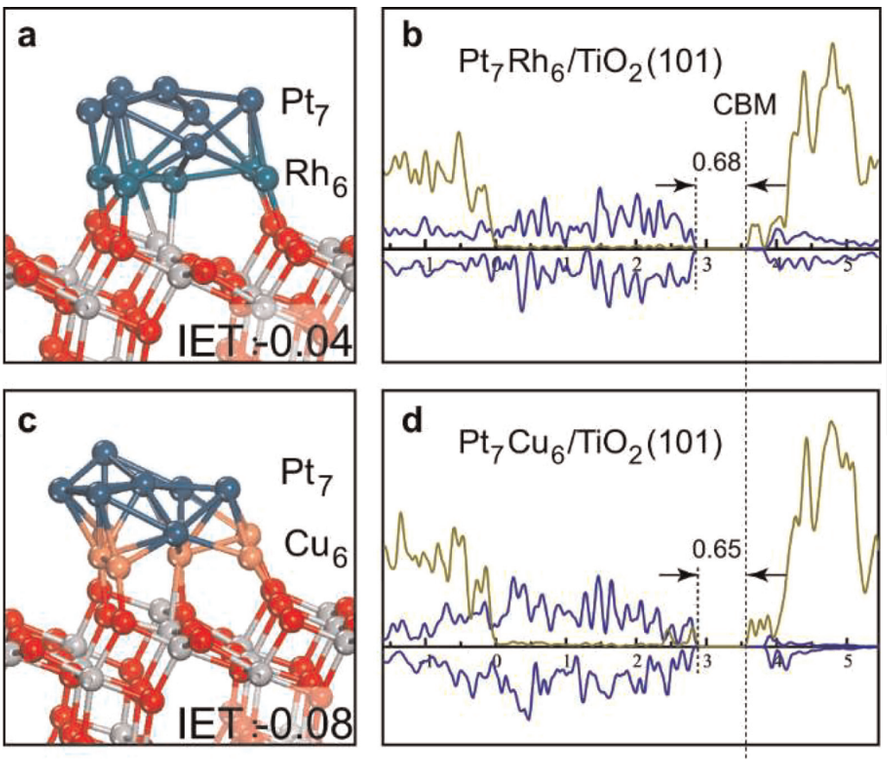

Figure 10.
Optimal models (a, c) for electron transfer between TiO2 (1 0 1) anatase surface and alloyed metal cocatalysts, proposed by Wang and Gong and their corresponding density of states distribution (b, d). In images (b, d), blue line shows the states of the metal cluster, while yellow-green is TiO2. Reprinted from the [92] under a creative commons attribution 4.0 international license. IET refers to the energy of intrinsic electron transfer in eV.

importance of optimizing facet-facet exposition and further facet-co-catalyst interactions to optimize the final performance.

Furthermore, recent studies also focus on the photocatalytic reduction of carbon (IV) oxide to valuable chemical compounds. This reaction begins with the adsorption of CO_2 and H_2O molecules, which was investigated theoretically by Mishra and Nanda. Using DFT calculations, they examined the chemical restructuring of CO_2 and H_2O molecules during the process of adsorption, co-adsorption, and conversion on (0 0 1), (1 0 0), and (1 0 1) surfaces [85]. They observed that the energy barrier of bicarbonate complex formation, which resulted from the co-adsorption of carbon dioxide and water, was the lowest for the (0 0 1) surface. Therefore, {0 0 1} facets are supposed to be the most reactive anatase facets for CO_2 photocatalytic reduction. However, if this surface undergoes reconstruction, the number of active sites is reduced. Therefore, experimental conditions like temperature and high vacuum will be crucial for the photocatalytic performance of anatase nanocrystals.

Although the photocatalytic reaction depends on the adsorption of reactants, the investigations provided by Ma et al., in the application of CO_2 reduction to formic acid, showed different behavior of anatase crystal facets compared with previous studies [86]. The surface electron transfer for (0 0 1) and (1 0 1) surfaces was characterized by similar barrier levels. However, the reductive ability of electrons generated on the (1 0 1) plane is higher than that on the (0 0 1) plane; therefore, electrons may be transferred more easily to reactants for low-energetic facets. Moreover, HCOOH on the (0 0 1) surface can replace water and, in consequence, occupy the active sites, hindering the reaction. On the contrary, formic acid seemed to remain undissociated on (1 0 1) surfaces, so more suitable product adsorption properties led to a higher photocatalytic performance.

The above-reported studies were theoretical, so the experimental results may not be consistent with DFT calculations. Therefore, Liu et al. demonstrated the blue anatase nanocrystals with exposed {0 0 1}, {1 0 1}, and a combination of {1 0 1} and {0 0 1} facets [87]. They reported that oxygen-deficient TiO_2 nanostructures with co-exposed {1 0 1} and {0 0 1} facets exhibited relatively high quantum yield for CO_2 reduction to CO (0.31% under UV–vis light and 0.134% under visible light). Moreover, this photocatalyst demonstrated more than four times higher visible light activity in comparison with {0 0 1} or {1 0 1}. This high photocatalytic activity was a result of two effects. Firstly, co-exposed {0 0 1} and {1 0 1} facets had increased the capacity of reversible CO_2 adsorption. Secondly, the created surface junction between facets enhanced the charge separation and hindered the recombination processes. Similar results were obtained by Yu et al., who investigated the mist-efficient content ratio of {0 0 1} and {1 0 1} facets [88]. The decahedral-shaped sample with 58% content of {0 0 1} facets exhibited the highest methane production from CO_2. {1 0 1} facets acted as reduction sites, whereas {0 0 1} facets were the oxidation sites on the photocatalyst surface. However, a too high amount of the {0 0 1} facets on the anatase surface may have caused an electron overflow effect toward {1 0 1} facets, so the migration of electrons to {1 0 1} facets is more difficult than in the previous case.

Carbon dioxide may be further converted to methane, which generally gives rise to operational risks and environmental problems [89, 90]. Therefore, selective oxidation to CH_3OH is a promising way to CH_4 storage. Feng et al. reported the facet-dependent selectivity of $CH_4 \rightarrow CH_3OH$ conversion over anatase nanocrystals. They showed that silver-decorated TiO_2 with predominant {0 0 1} facets exhibited a selectivity of approximately 80%, which was significantly better than the sample with dominated {1 0 1} facets. This high selectivity resulted from oxygen vacancy generation by

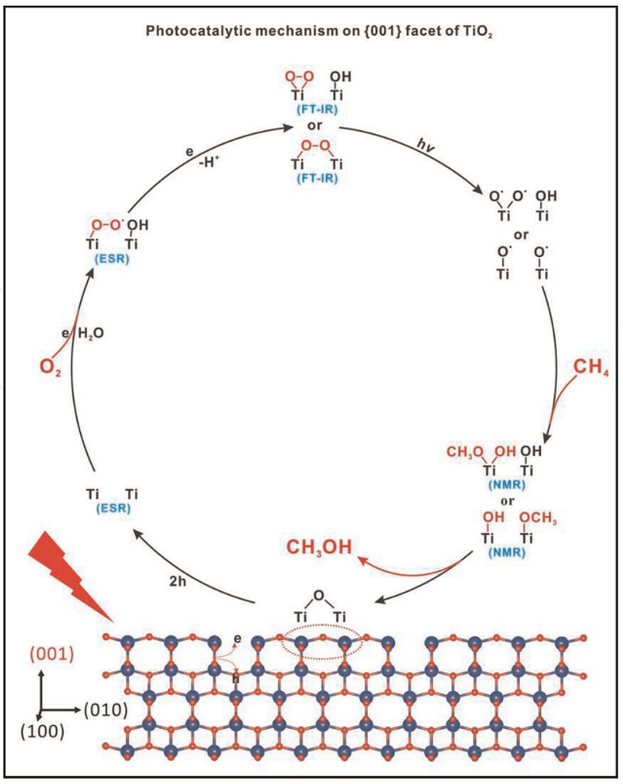

Figure 11.
The proposed mechanism of methane photocatalytic conversion over {0 0 1} anatase crystal facet. Reprinted from [101] under a creative commons attribution 4.0 international license.

photoinduced holes, which played a crucial role in avoiding the formation of $\cdot CH_3$ and $\cdot OH$ radicals. Therefore, the undesired overoxidation to CO was limited, in opposite to TiO_2 exposing {1 0 1} facets [91]. The proposed mechanism of CH_4 oxidation on the {0 0 1} facets is presented in **Figure 11**.

5. Conclusions

The surface structure of TiO_2 is constantly being recognized as a crucial factor regarding its photocatalytic activity. Control over this interface can be achieved by exposing the specific crystal facets, which allows detailed insight into the reaction kinetics and mechanism. Experimentally, such high-quality structures can be prepared through energetic stabilization of the specific facet, with simultaneous control of nucleation and growth rates. However, contrary to the preparation procedures, surface energy is now recognized as a less important factor for the final photocatalytic activity. Here, more attention is given to the electronic properties, detailed interactions with substrates, and local defects. However, as the presented chapter aimed to provide a general introduction to the problem of TiO_2 facets, only some of the recent findings were stressed here, while these problems are still under constant intensive research. Particularly, it should be highlighted that further modifications and charge separation between different co-exposed facets are now used to achieve remarkable final photocatalytic efficiency of different materials. In this regard, we believe that the presented findings will be useful for further studies in this direction, providing a survey of different aspects of crystal facet engineering of TiO_2, a photocatalyst that is still the most studied in this field.

Acknowledgements

The research was financially supported by the Polish National Science Centre grant no. NCN 2021/43/B/ST5/02983.

Author details

Szymon Dudziak, Marta Kowalkińska and Anna Zielińska-Jurek*
Department of Process Engineering and Chemical Technology, Gdansk University of Technology, Gdansk, Poland

*Address all correspondence to: annjurek@pg.edu.pl

References

[1] Gerischer H, Heller A. The role of oxygen in photooxidation of organic molecules on semiconductor particles. The Journal of Physical Chemistry. 1991; **95**(13):5261-5267

[2] Wang CM, Heller A, Gerischer H. Palladium catalysis of O_2 reduction by electrons accumulated on TiO2 particles during Photoassisted oxidation of organic compounds. Journal of the American Chemical Society. 1992; **114**(13):5230-5234

[3] Moser J, Punchihewa S, Infelta PP, Grätzel M. Surface complexation of colloidal semiconductors strongly enhances interfacial electron-transfer rates. Langmuir. 1991;**7**(12): 3012-3018

[4] Takata T, Jiang J, Sakata Y, Nakabayashi M, Shibata N, Nandal V, et al. Photocatalytic water splitting with a quantum efficiency of almost unity. Nature. 2020;**581**(7809): 411-414

[5] Lazzeri M, Vittadini A, Selloni A. Structure and energetics of stoichiometric TiO_2 anatase surfaces. Physical Review B - Condensed Matter and Materials Physics. 2001;**63**(15): 1554091-1554099

[6] Zhao Z, Li Z, Zou Z. Surface properties and electronic structure of low-index stoichiometric anatase TiO_2 surfaces. Journal of Physics. Condensed Matter. 2010;**22**(17):175008

[7] Arrouvel C, Digne M, Breysse M, Toulhoat H, Raybaud P. Effects of morphology on surface hydroxyl concentration: A DFT comparison of anatase-TiO_2 and γ-alumina catalytic supports. Journal of Catalysis. 2004; **222**(1):152-166

[8] Lazzeri M, Selloni A. Stress-driven reconstruction of an oxide surface: The anatase TiO_2 (001)-(1×4) surface. Physical Review Letters. 2001;**87**(26): 266105-1-266105-4

[9] Mino L, Ferrari AM, Lacivita V, Spoto G, Bordiga S, Zecchina A. CO adsorption on anatase nanocrystals: A combined experimental and periodic DFT study. Journal of Physical Chemistry C. 2011;**115**(15): 7694-7700

[10] Labat F, Baranek P, Adamo C. Structural and electronic properties of selected rutile and anatase TiO_2 surfaces: An ab initio investigation. Journal of Chemical Theory and Computation. 2008;**4**(2):341-352

[11] Barnard AS, Curtiss LA. Prediction of TiO_2 nanoparticle phase and shape transitions controlled by surface chemistry. Nano Letters. 2005;**5**(7): 1261-1266

[12] Perron H, Domain C, Roques J, Drot R, Simoni E, Catalette H. Optimisation of accurate rutile TiO_2 (110), (100), (101) and (001) surface models from periodic DFT calculations. Theoretical Chemistry Accounts. 2007; **117**(4):565-574

[13] Jiang F, Yang L, Zhou D, He G, Zhou J, Wang F, et al. First-principles atomistic Wulff constructions for an equilibrium rutile TiO_2 shape modeling. Applied Surface Science. 2018;**436**: 989-994

[14] Ramamoorthy M, Vanderbilt D, King-Smith RD. First-principles calculations of the energetics of stoichiometric TiO_2 surfaces. Physical Review B. 1994;**49**(23): 16721-16727

[15] Gong XQ, Selloni A. First-principles study of the structures and energetics of stoichiometric brookite TiO_2 surfaces. Physical Review B. Condensed Matter and Materials Physics. 2007;**76**(23):1-11

[16] Lin H, Li L, Zhao M, Huang X, Chen X, Li G, et al. Synthesis of high-quality brookite TiO_2 single-crystalline nanosheets with specific facets exposed: Tuning catalysts from inert to highly reactive. Journal of the American Chemical Society. 2012;**134**(20): 8328-8331

[17] Jiang HB, Cuan Q, Wen CZ, Xing J, Wu D, Gong XQ, et al. Anatase TiO_2 crystals with exposed high-index facets. Angewandte Chemie - International Edition. 2011;**50**(16):3764-3768

[18] Wang Y, Sun T, Liu X, Zhang H, Liu P, Yang H, et al. Geometric structure of rutile titanium dioxide (111) surfaces. Physical Review B. Condensed Matter and Materials Physics. 2014;**90**(4):1-6

[19] Zhou G, Jiang L, Dong Y, Li R, He D. Engineering the exposed facets and open-coordinated sites of brookite TiO_2 to boost the loaded Ru nanoparticle efficiency in benzene selective hydrogenation. Applied Surface Science. 2019;**486**:187-197

[20] Hengerer R, Bolliger B, Erbudak M, Grätzel M. Structure and stability of the anatase TiO_2 (101) and (001) surfaces. Surface Science. 2000;**460**(1–3):162-169

[21] Liang Y, Gan S, Chambers SA, Altman EI. Surface structure of anatase (001) reconstruction, atomic steps, and domains. Physical Review B. Condensed Matter and Materials Physics. 2001; **63**(23):1-7

[22] Herman GS, Sievers MR, Gao Y. Structure determination of the two-Domain (1 x 4) Anatase TiO_2 (001) surface. Physical Review Letters. 2000; **84**:3354

[23] Wang Y, Sun H, Tan S, Feng H, Cheng Z, Zhao J, et al. Role of point defects on the reactivity of reconstructed anatase titanium dioxide (001) surface. Nature Communications. 2013;**4**:1-8

[24] Selçuk S, Selloni A. Surface structure and reactivity of anatase TiO_2 crystals with dominant {001} facets. Journal of Physical Chemistry C. 2013;**117**(12): 6358-6362

[25] Yuan W, Wang Y, Li H, Wu H, Zhang Z, Selloni A, et al. Real-time observation of reconstruction dynamics on TiO_2 (001) surface under oxygen via an environmental transmission electron microscope. Nano Letters. 2016;**16**(1): 132-137

[26] Yang HG, Sun CH, Qiao SZ, Zou J, Liu G, Smith SC, et al. Anatase TiO_2 single crystals with a large percentage of reactive facets. Nature. 2008;**453**(7195): 638-641

[27] DeBenedetti WJI, Skibinski ES, Jing D, Song A, Hines MA. Atomic-scale understanding of catalyst activation: Carboxylic acid solutions, but not the acid itself, increase the reactivity of Anatase (001) faceted Nanocatalysts. Journal of Physical Chemistry C. 2018; **122**(8):4307-4314

[28] Wang Y, Lee S, Vilmercati P, Lee HN, Weitering HH, Snijders PC. Atomically flat reconstructed rutile TiO_2 (001) surfaces for oxide film growth. Applied Physics Letters. 2016;**108**(9): 091604

[29] Tait RH, Kasowski RV. Ultraviolet photoemission and low-energy-electron diffraction studies of TiO_2 (rutile) (001) and (110) surfaces. Physical Review B. 1979;**20**(12):5178-5191

[30] Firment LE. Thermal faceting of the rutile TiO_2 (001) surface. Surface Science. 1982;**116**(2):205-216

[31] Zhou R, Li D, Qu B, Sun X, Zhang B, Zeng XC. Rutile TiO_2 (011)-2 × 1 reconstructed surfaces with optical absorption over the visible light Spectrum. ACS Applied Materials & Interfaces. 2016;**8**(40):27403-27410

[32] Wu L, Wang Z, Xiong F, Sun G, Chai P, Zhang Z, et al. Surface chemistry and photochemistry of small molecules on rutile TiO_2 (001) and TiO_2 (011)-(2 × 1) surfaces: The crucial roles of defects. The Journal of Chemical Physics. 2020;**152**:044702

[33] Gong XQ, Khorshidi N, Stierle A, Vonk V, Ellinger C, Dosch H, et al. The 2 × 1 reconstruction of the rutile TiO2(0 1 1) surface: A combined density functional theory, X-ray diffraction, and scanning tunneling microscopy study. Surface Science. 2009;**603**:138-144

[34] Balzaretti F, Gupta V, Ciacchi LC, Aradi B, Frauenheim T, Köppen S. Water reactions on reconstructed rutile TiO_2: A density functional theory/density functional tight binding approach. Journal of Physical Chemistry C. 2021;**125**(24):13234-13246

[35] Wulff G. Zur Frage der Geschwindigkeit des Wachsthums und der Auflösung der Krystallflächen. Zeitschrift für Krystallographie und Mineralogie. 1901;**34**:449-530

[36] Huang Z, Wang Z, Lv K, Zheng Y, Deng K. Transformation of $TiOF_2$ cube to a hollow nanobox assembly from anatase TiO_2 nanosheets with exposed {001} facets via solvothermal strategy. ACS Applied Materials & Interfaces. 2013;**5**(17):8663-8669

[37] Dudziak S, Kowalkińska M, Karczewski J, Pisarek M, Siuzdak K, Kubiak A, et al. Solvothermal growth of {0 0 1} exposed anatase nanosheets and their ability to mineralize organic pollutants. The effect of alcohol type and content on the nucleation and growth of TiO_2 nanostructures. Applied Surface Science. 2021;**563**:150360

[38] Amano F, Yasumoto T, Prieto-Mahaney OO, Uchida S, Shibayama T, Ohtani B. Photocatalytic activity of octahedral single-crystalline mesoparticles of anatase titanium(IV) oxide. Chemical Communications. 2009; **17**:2311-2313

[39] Li J, Yu Y, Chen Q, Li J, Xu D. Controllable synthesis of TiO_2 single crystals with tunable shapes using ammonium-exchanged titanate nanowires as precursors. Crystal Growth & Design. 2010;**10**(5):2111-2115

[40] Lai Z, Peng F, Wang Y, Wang H, Yu H, Liu P, et al. Low temperature solvothermal synthesis of anatase TiO_2 single crystals with wholly {100} and {001} faceted surfaces. Journal of Materials Chemistry. 2012;**22**(45): 23906-23912

[41] Kowalkińska M, Dudziak S, Karczewski J, Ryl J, Trykowski G, Zielińska-Jurek A. Facet effect of TiO_2 nanostructures from $TiOF_2$ and their photocatalytic activity. Chemical Engineering Journal. 2021;**404**:126493

[42] Gai L, Mei Q, Qin X, Li W, Jiang H, Duan X. Controlled synthesis of anatase TiO_2 octahedra with enhanced photocatalytic activity. Materials Research Bulletin. 2013;**48**: 4469-4475

[43] Wang F, Sun L, Li Y, Zhan W, Wang X, Han X. Hollow Anatase TiO_2 Octahedrons with Exposed High-Index

{102} Facets for Improved Dye-Sensitized Photoredox Catalysis Activity. Inorganic Chemistry. 2018;**57**(8): 4550-4555

[44] Xu H, Ouyang S, Li P, Kako T, Ye J. High-active anatase TiO_2 nanosheets exposed with 95% {100} facets toward efficient H_2 evolution and CO_2 photoreduction. ACS Applied Materials & Interfaces. 2013;**5**(4):1348-1354

[45] Li J, Xu D. Tetragonal faceted-nanorods of anatase TiO_2 single crystals with a large percentage of active {100} facets. Chemical Communications. 2010; **46**(13):2301-2303

[46] Wen CZ, Zhou JZ, Jiang HB, Hu QH, Qiao SZ, Yang HG. Synthesis of micro-sized titanium dioxide nanosheets wholly exposed with high-energy {001} and {100} facets. Chemical Communications. 2011;**47**(15): 4400-4402

[47] Yang HG, Liu G, Qiao SZ, Sun CH, Jin YG, Smith SC, et al. Solvothermal synthesis and photoreactivity of anatase TiO2 nanosheets with dominant {001} facets. Journal of the American Chemical Society. 2009;**131**(11):4078-4083

[48] Zheng Y, Wang J, Yang P. Anatase TiO_2 nanosheets exposed {001} facet: Solvent effects on the photocatalytic performance. Journal of Nanoscience and Nanotechnology. 2017;**17**(2): 1204-1209

[49] Li Q, Li T, Chang S, Tao Q, Tian B, Zhang J. Enlarging {110} exposed facets of anatase TiO_2 by the synergistic action of capping agents. Cryst Eng Comm. 2016;**18**(27):5074-5078

[50] Xu H, Reunchan P, Ouyang S, Tong H, Umezawa N, Kako T, et al. Anatase TiO_2 single crystals exposed with high-reactive {111} facets toward efficient H_2 evolution. Chemistry of Materials. 2013;**25**(3):405-411

[51] Lai Z, Peng F, Wang H, Yu H, Zhang S, Zhao H. A new insight into regulating high energy facets of rutile TiO_2. Journal of Materials Chemistry A. 2013;**1**(13):4182-4185

[52] Kobayashi M, Petrykin V, Kakihana M, Tomita K. Hydrothermal synthesis and photocatalytic activity of whisker-like rutile-type titanium dioxide. Journal of the American Ceramic Society. 2009;**92**:S21-S26

[53] Wu T, Kang X, Kadi MW, Ismail I, Liu G, Cheng HM. Enhanced photocatalytic hydrogen generation of mesoporous rutile TiO_2 single crystal with wholly exposed {111} facets. Chinese Journal of Catalysis. 2015;**36**: 2103-2108

[54] Truong QD, Hoa HT, Le TS. Rutile TiO_2 nanocrystals with exposed {3 3 1} facets for enhanced photocatalytic CO_2 reduction activity. Journal of Colloid and Interface Science. 2017;**504**:223-229

[55] Chen JS, Lou XW. Unusual rutile TiO_2 nanosheets with exposed (001) facets. Chemical Science. 2011;**2**(11): 2219-2223

[56] Perego C, Wang YH, Durupthy O, Cassaignon S, Revel R, Jolivet JP. Nanocrystalline brookite with enhanced stability and photocatalytic activity: Influence of lanthanum (III) doping. ACS Applied Materials & Interfaces. 2012;**4**(2):752-760

[57] Xu Y, Lin H, Li L, Huang X, Li G. Precursor-directed synthesis of well-faceted brookite TiO_2 single crystals for efficient photocatalytic performances. Journal of Materials Chemistry A. 2015; **3**(44):22361-22368

[58] Shi T, Duan Y, Lv K, Hu Z, Li Q, Li M, et al. Photocatalytic oxidation of acetone over high thermally stable TiO_2 nanosheets with exposed (001) facets. Frontiers in Chemistry. 2018;**6**(MAY): 1-10

[59] Liu M, Piao L, Zhao L, Ju S, Yan Z, He T, et al. Anatase TiO_2 single crystals with exposed {001} and {110} facets: Facile synthesis and enhanced photocatalysis. Chemical Communications. 2010;**46**(10): 1664-1666

[60] Zhao M, Xu H, Chen H, Ouyang S, Umezawa N, Wang D, et al. Photocatalytic reactivity of {121} and {211} facets of brookite TiO_2 crystals. Journal of Materials Chemistry A. 2015; **3**(5):2331-2337

[61] Pan J, Liu G, Lu GQ, Cheng HM. On the true photoreactivity order of {001}, {010}, and {101} facets of anatase TiO_2 crystals. Angewandte Chemie - International Edition. 2011;**50**(9): 2133-2137

[62] Ye L, Mao J, Peng T, Zan L, Zhang Y. Opposite photocatalytic activity orders of low-index facets of anatase TiO_2 for liquid phase dye degradation and gaseous phase CO_2 photoreduction. Physical Chemistry Chemical Physics. 2014;**16**(29):15675-15680

[63] Mao J, Ye L, Li K, Zhang X, Liu J, Peng T, et al. Pt-loading reverses the photocatalytic activity order of anatase TiO_2 {001} and {010} facets for photoreduction of CO_2 to CH_4. Applied Catalysis B: Environmental. 2014;**144**: 855-862

[64] Li M, Chen Y, Li W, Li X, Tian H, Wei X, et al. Ultrathin anatase TiO_2 nanosheets for high-performance photocatalytic hydrogen production. Small. 2017;**13**(16):1604115

[65] Xiang Q, Lv K, Yu J. Pivotal role of fluorine in enhanced photocatalytic activity of anatase TiO_2 nanosheets with dominant (0 0 1) facets for the photocatalytic degradation of acetone in air. Applied Catalysis B: Environmental. 2010;**96**(3–4):557-564

[66] Wu Q, Liu M, Wu Z, Li Y, Piao L. Is photooxidation activity of {001} facets truly lower than that of {101} facets for anatase TiO_2 crystals? Journal of Physical Chemistry C. 2012;**116**(51):26800-26804

[67] Gordon TR, Cargnello M, Paik T, Mangolini F, Weber RT, Fornasiero P, et al. Nonaqueous synthesis of TiO_2 nanocrystals using TiF_4 to engineer morphology, oxygen vacancy concentration, and photocatalytic activity. Journal of the American Chemical Society. 2012;**134**(15): 6751-6761

[68] Mino L, Pellegrino F, Rades S, Radnik J, Hodoroaba VD, Spoto G, et al. Beyond Shape Engineering of TiO_2 Nanoparticles: Post-Synthesis Treatment Dependence of Surface Hydration, Hydroxylation, Lewis Acidity and Photocatalytic Activity of TiO2 Anatase Nanoparticles with Dominant {001} or {101} Facets. ACS Applied Nano Materials. 2018;**1**(9):5355-5365

[69] Günnemann C, Haisch C, Fleisch M, Schneider J, Emeline AV, Bahnemann DW. Insights into different photocatalytic oxidation activities of Anatase, Brookite, and rutile single-crystal facets. ACS Catalysis. 2019;**9**(2): 1001-1012

[70] Amalia FR, Takashima M, Ohtani B. Are you still using organic dyes? Colorimetric formaldehyde analysis for true photocatalytic-activity evaluation. Chemical Communications. 2022;**58**: 11721-11724

[71] Agrios AG, Pichat P. Recombination rate of photogenerated charges versus surface area: Opposing effects of TiO_2 sintering temperature on photocatalytic removal of phenol, anisole, and pyridine in water. Journal of Photochemistry and Photobiology A: Chemistry. 2006;**180**(1–2):130-135

[72] Lv K, Guo X, Wu X, Li Q, Ho W, Li M, et al. Photocatalytic selective oxidation of phenol to produce dihydroxybenzenes in a TiO_2/UV system: Hydroxyl radical versus hole. Applied Catalysis B: Environmental. 2016;**199**:405, 405-411, 411. DOI: 10.1016/j.apcatb.2016.06.049

[73] Bahnemann DW, Hilgendorff M, Memming R. Charge carrier dynamics at TiO_2 particles: Reactivity of free and trapped holes. The Journal of Physical Chemistry. A. 1997;**101**(21):4265-4275

[74] Ma X, Dai Y, Guo M, Huang B. Relative photooxidation and photoreduction activities of the {100}, {101}, and {001} Surfaces of Anatase TiO_2. Langmuir. 2013;**29**(44): 13647-13654

[75] Antunes CSA, Bietti M, Salamone M, Scione N. Early stages in the TiO_2-photocatalyzed degradation of simple phenolic and non-phenolic lignin model compounds. Journal of Photochemistry and Photobiology A: Chemistry. 2004; **163**(3):453-462

[76] Setvin M, Aschauer U, Hulva J, Simschitz T, Daniel B, Schmid M, et al. Following the reduction of oxygen on TiO_2 Anatase (101) step by step. Journal of the American Chemical Society. 2016; **138**(30):9565-9571

[77] Chen J, Li YF, Sit P, Selloni A. Chemical dynamics of the first proton-coupled electron transfer of water oxidation on TiO_2 anatase. Journal of the American Chemical Society. 2013; **135**(50):18774-18777

[78] Hwang JY, Hee MG, Kim B, Tachikawa T, Majima T, Hong S, et al. Crystal phase-dependent generation of mobile OH radicals on TiO_2: Revisiting the photocatalytic oxidation mechanism of anatase and rutile. Applied Catalysis B: Environmental. 2021;**November 2020**(286):119905

[79] Dudziak S, Kowalkińska M, Karczewski J, Pisarek M, Gouveia JD, Gomes JRB, et al. Surface and trapping energies as predictors for the photocatalytic degradation of aromatic organic pollutants. Journal of Physical Chemistry C. 2022;**126**: 14859-14877

[80] Kowalkińska M, Sikora K, Łapiński M, Karczewski J, Zielińska-Jurek A. Non-toxic fluorine-doped TiO_2 nanocrystals from $TiOF_2$ for facet-dependent naproxen degradation. Catalysis Today. 2022;**413–415**:113959

[81] Wang Y, Mino L, Pellegrino F, Homs N, Ramírez de la Piscina P. Engineered MoxC/TiO_2 interfaces for efficient noble metal-free photocatalytic hydrogen production. Applied Catalysis B: Environmental. 2022;**318**:121783

[82] Wang D, Gong XQ. Function-oriented design of robust metal cocatalyst for photocatalytic hydrogen evolution on metal/titania composites. Nature Communications. 2021;**12**:1-6

[83] Wei Z, Janczarek M, Endo M, Wang K, Balčytis A, Nitta A, et al. Noble metal-modified faceted anatase titania photocatalysts: Octahedron versus decahedron. Applied Catalysis B: Environmental. 2018;**237**:574-587

[84] Meng A, Zhang J, Xu D, Cheng B, Yu J. Enhanced photocatalytic H_2-

production activity of anatase TiO_2 nanosheet by selectively depositing dual-cocatalysts on (101) and (001) facets. Applied Catalysis B: Environmental. 2016;**198**:286-294

[85] Mishra SB, Nanda BRK. Facet dependent catalytic activities of anatase TiO_2 for CO2 adsorption and conversion. Applied Surface Science. 2020;**531**:147330

[86] Ma S, Song W, Liu B, Zhong W, Deng J, Zheng H, et al. Facet-dependent photocatalytic performance of TiO_2: A DFT study. Applied Catalysis B: Environmental. 2016;**198**:1-8

[87] Liu L, Jiang Y, Zhao H, Chen J, Cheng J, Yang K, et al. Engineering Coexposed {001} and {101} Facets in Oxygen-Deficient TiO_2 Nanocrystals for Enhanced CO2 Photoreduction under Visible Light. ACS Catalysis. 2016;**6**(2): 1097-1108

[88] Yu J, Low J, Xiao W, Zhou P, Jaroniec M. Enhanced Photocatalytic CO_2-Reduction Activity of Anatase TiO2 by Co-exposed {001} and {101} Facets. Journal of the American Chemical Society. 2014;**136**:8839

[89] Keller N, Ivanez J, Highfield J, Ruppert AM. Photo−/thermal synergies in heterogeneous catalysis: Towards low-temperature (solar-driven) processing for sustainable energy and chemicals. Applied Catalysis B: Environmental. 2021;**296**:120320

[90] Fang F, Liu Y, Sun X, Fu C, Prakash Bhoi Y, Xiong W, et al. TiO2 facet-dependent reconstruction and photocatalysis of CuOx/TiO_2 photocatalysts in CO_2 photoreduction. Applied Surface Science. 2021;**564**:150407

[91] Feng N, Lin H, Song H, Yang L, Tang D, Deng F, et al. Efficient and selective photocatalytic CH_4 conversion to CH_3OH with O_2 by controlling overoxidation on TiO_2. Nature Communications. 2021;**12**(1):4652